MOLECULAR AND CELLULAR BIOLOGY, Apr. 2008, p. 2675–2689 Vol. 28, No. 8
0270-7306/08/$08.00+0 doi:10.1128/MCB.01945-07

Identification of ZBP-89 as a Novel GATA-1-Associated Transcription Factor Involved in Megakaryocytic and Erythroid Development▽†

Andrew J. Woo,[1] Tyler B. Moran,[1] Yocheved L. Schindler,[1] Seong-Kyu Choe,[2] Nathaniel B. Langer,[2] Matthew R. Sullivan,[1] Yuko Fujiwara,[1] Barry H. Paw,[2] and Alan B. Cantor[1]*

Department of Pediatric Oncology, Children's Hospital Boston/Dana Farber Cancer Institute, Harvard Medical School, Boston, Massachusetts 02115,[1] and Division of Hematology, Brigham and Women's Hospital, Harvard Medical School, Boston, Massachusetts 02115[2]

Received 29 October 2007/Returned for modification 16 December 2007/Accepted 24 January 2008

A complete understanding of the transcriptional regulation of developmental lineages requires that all relevant factors be identified. Here, we have taken a proteomic approach to identify novel proteins associated with GATA-1, a lineage-restricted zinc finger transcription factor required for terminal erythroid and megakaryocytic maturation. We identify the Krüppel-type zinc finger transcription factor ZBP-89 as being a component of multiprotein complexes involving GATA-1 and its essential cofactor Friend of GATA-1 (FOG-1). Using chromatin immunoprecipitation assays, we show that GATA-1 and ZBP-89 cooccupy *cis*-regulatory elements of certain erythroid and megakaryocyte-specific genes, including an enhancer of the GATA-1 gene itself. Loss-of-function studies in zebrafish and mice demonstrate an in vivo requirement for ZBP-89 in megakaryopoiesis and definitive erythropoiesis but not primitive erythropoiesis, phenocopying aspects of FOG-1- and GATA-1-deficient animals. These findings identify ZBP-89 as being a novel transcription factor involved in erythroid and megakaryocytic development and suggest that it serves a cooperative function with GATA-1 and/or FOG-1 in a developmental stage-specific manner.

Lineage-specific transcription factors play essential roles in development. However, most of these factors have relatively small consensus DNA binding motifs, and by themselves, they are not likely to account for high-fidelity lineage-specific gene expression in higher organisms. Indeed, recent studies employing chromatin immunoprecipitation (IP) (ChIP) across extended loci or entire genomes show that only a small percentage of consensus binding sites, as defined by in vitro methods, are occupied by a given transcription factor in vivo (4, 7). Conversely, transcription factor chromatin occupancy has been documented in regions containing only low-affinity sites (23). Although chromatin accessibility likely plays a role in some of this site selectivity, considerable evidence for combinatorial transcription factor binding mechanisms exists. Therefore, a more complete understanding of eukaryotic transcription factor binding in vivo requires that all relevant transcription factors for a given developmental lineage be identified.

GATA family transcription factors play essential roles in diverse developmental settings. There are six known GATA genes (GATA-1, -2, -3, -4, -5, and -6) in vertebrates, each having distinct and, in some cases, overlapping patterns of expression. All vertebrate GATA factors contain two closely spaced zinc fingers, which share high amino acid sequence conservation among the different members. The carboxyl zinc finger mediates high-affinity binding to the consensus sequence (T/A)GATA(A/G), whereas the amino zinc finger stabilizes the interaction at certain double GATA sites (51).

GATA-1 was first identified as being a protein that binds to key DNA *cis*-regulatory elements within the α- and β-globin loci in erythroid cells (18, 52). Since then, GATA-1 has been shown to control the expression of many genes involved in erythroid maturation and to be required for normal erythroid development in vivo (19, 61). GATA-1 is also highly expressed in megakaryocytic cells, the precursors of blood platelets, where it controls the expression of multiple megakaryocyte-specific genes (37). Mice containing a megakaryocyte-selective GATA-1 deficiency have hyperproliferative megakaryocytes that are blocked at a relatively late stage of maturation (48, 56). Acquired GATA-1 mutations that lead to the exclusive production of a short isoform (GATA-1s) are highly associated with a transient neonatal myeloproliferative disorder and subsequent acute megakaryoblastic leukemia in children with Down syndrome (38).

The amino zinc finger of GATA factors interacts with Friend of GATA (FOG) proteins, a family of large multitype zinc finger transcriptional cofactors (6). There are two known FOG genes in mammals: FOG-1, which is expressed predominantly within the hematopoietic system, and FOG-2, which is present in most nonhematopoietic tissues. All six GATA factors bind FOG-1 or FOG-2 in vitro. Like GATA-1^{-} male mice (GATA-1 is located on the X chromosome in mice and humans), FOG-1$^{-/-}$ mice die between embryonic day 10.5 (E10.5) and E12.5 from severe anemia due to a block in erythroid maturation at a proerythroblast-like stage (19, 53). However, in contrast to GATA-1^{-} animals, FOG-1$^{-/-}$ embryos exhibit a complete failure of megakaryopoiesis. This discrepancy is explained by the overlapping FOG-1-dependent roles of GATA-1 and GATA-2, another hematopoietic expressed GATA factor, during early stages of megakaryopoiesis (8).

* Corresponding author. Mailing address: 300 Longwood Ave., Karp 7, Children's Hospital Boston, Boston, MA 02115. Phone: (617) 919-2026. Fax: (617) 730-0222. E-mail: alan.cantor@childrens.harvard.edu.

† Supplemental material for this article may be found at http://mcb.asm.org/.

▽ Published ahead of print on 4 February 2008.

A direct physical interaction between GATA and FOG family proteins is required for normal hematopoietic, cardiac, and gonadal development in vivo (8, 10, 39, 50). Despite the critical role that FOG proteins play in GATA factor function, their mechanism of action remains incompletely understood. As of yet, no sequence-specific, high-affinity DNA binding activity of FOG proteins has been demonstrated, implying that they function via protein-protein interactions. ChIP studies demonstrate the FOG-1 facilitation of GATA-1 chromatin occupancy in a gene context-dependent manner (30, 40). However, the mechanisms underlying this activity and the basis for its site selectivity are unknown.

In this study, we report the identification of ZBP-89, a Krüppel-type GC-rich binding transcription factor, as a novel GATA-1-associated protein and show that it is required for normal megakaryocytic and definitive erythroid development in vitro and in vivo. Gel filtration and coimmunoprecipitation (co-IP) experiments suggest the participation of ZBP-89 in a common complex with GATA-1 and FOG-1, and loss-of-function studies show phenocopying of ZBP-89 and FOG-1 deficiency in early megakaryopoiesis. We propose that ZBP-89 plays a cooperative role with GATA-1 and FOG-1, contributing to a high-affinity, site-selective DNA binding complex.

MATERIALS AND METHODS

Plasmid construction. Standard recombinant DNA techniques were used for all molecular cloning procedures (46). pEFBirA-V5-His was generated by inserting the cDNA for *Escherichia coli birA* into the BamHI/XbaI sites of pEF1/V5-HisA (Invitrogen). The sequence 5′-CGCCAGCC-3′ was inserted between the BamHI site and the first codon to optimize translation in eukaryotic cells. The biotin-tagging vector pEF-Biotag was created by cloning the BirA recognition coding sequence from pAN-4 (Avidity) (5′-GGGTCCGGCCTGAACGAC ATCTTCGAGGCTCAGAAAATCGAATGGCACGAAGGCGCGCCGAGC TCGAGGATC-3′) into the SmaI/BamHI sites of pEFFLAGpgkpuropA (25). The cDNA for murine GATA-1 was then subcloned into the BamHI/XbaI sites to generate pEF-FLAG-Bio-GATA-1. For co-IP and mapping experiments, the cDNA for rat ZBP-89 (34) or selected domains was cloned into the NotI/XbaI sites of pEF1/V5-HisA (Invitrogen). cDNAs encoding full-length murine GATA-1, domains of murine GATA-1, or full-length human GATA-2 were cloned into the BamHI/XbaI sites of pEF-FLAGpgkpuropA. For retroviral expression, the cDNA encoding rat ZBP-89 was cloned into the MluI/XhoI sites of MMP-HA-IRES-eGFP (5), and the enhanced green fluorescent protein (GFP) (eGFP) cassette was exchanged with a puromycin resistance gene cassette from pIRESpuro3 (Clontech).

Cell culture and transfection. Cell lines were cultured in 5% CO_2 at 37°C in media specific to the cell line, all supplemented with 100 U/ml of penicillin-streptomycin and 2 mM L-glutamine. The E14tg2A embryonic stem (ES) cell line was maintained in ES medium (Dulbecco's modified Eagle's medium) supplemented with 15% fetal calf serum (HyClone), 10^{-4} M 2-mercaptoethanol, 0.1 mM nonessential amino acids, 1% of nucleoside mix (100× stock; Sigma), and 1,000 U/ml recombinant leukemia inhibitory factor (Chemicon). COS-7 and mouse erythroleukemia (MEL) cells were cultured in Dulbecco's modified Eagle's low-glucose medium supplemented with 10% fetal calf serum. Erythrocyte differentiation of MEL cells was induced with 1.7% dimethyl sulfoxide. L8057 cells were cultured as previously described (26) and induced to differentiate with 50 nM 12-*O*-tetradecanoylphorbol-13-acetate (TPA; Sigma). G1E and G1ER cells were grown as previously described (21). β-Estradiol (Aldrich) was added to the medium at a final concentration of 10^{-7} M for induction experiments. L8057 and MEL cells (1×10^7 cells) were transfected with 20 μg of unlinearized plasmid using a Gene-Pulser II (Bio-Rad) apparatus set at 280 V and 975 μF. Stably transfected cells were selected with 0.5 mg/ml G418 and/or 2 μg/ml (L8057 cells) or 5 μg/ml (MEL cells) puromycin and cloned by limiting dilution. COS-7 cells were transfected using FuGene 6 reagent (Roche) according to the manufacturer's protocol.

GATA-1 multiprotein complex purification and proteomic analysis. L8057 and MEL clones stably expressing FLAG-biotin-tagged GATA-1 were induced with TPA (50 nM) for 3 days (L8057) or dimethyl sulfoxide (1.7%) for 1 day (MEL), and crude nuclear extracts were prepared from $\sim 1 \times 10^{10}$ cells essentially as described previously (12), except that mammalian protease inhibitor cocktail (Sigma) was added to buffers A and C at a 1:100 dilution. Nuclear extracts were immediately dialyzed against 50 volumes of BC139K buffer (139 mM KCl, 12 mM NaCl, 0.8 M $MgCl_2$, 20 mM Tris-HCl [pH 7.9], 0.5% NP-40, 0.2 mM EDTA, 20% [vol/vol] glycerol, 1 mM dithiothreitol, 0.2 mM phenylmethylsulfonyl fluoride, 0.1% mammalian protease inhibitor cocktail) at 4°C using a 10,000-molecular-weight-cutoff dialysis cassette (Pierce). The dialysate was centrifuged twice at 25,000 × *g* for 30 min at 4°C. Between 50 and 120 mg of total nuclear protein was then precleared with protein A/G beads (Roche) for 1 h on a rotating wheel at 4°C. The precleared supernatant was incubated with anti-FLAG M2-agarose beads (Sigma) overnight (14 to 16 h) on a rotating wheel. The beads were collected by centrifugation and washed four times with cold BC139K buffer on a rotating wheel at 4°C for 15 min each. Bound material was eluted by incubating beads in BC139K containing 0.1 mg/ml FLAG peptide (Sigma) for 90 min at 4°C on a rotating wheel. Material from four successive elutions was pooled and incubated with streptavidin-agarose beads (Invitrogen) for 14 to 16 h at 4°C on a rotating wheel. The beads were washed as described above, transferred into BC139 K buffer in which NaCl was substituted for KCl, and heated at 95°C to 100°C in Laemmli sodium dodecyl sulfate (SDS) sample buffer for 5 min. The eluted material was concentrated using a YM-10 Centricon (Millipore) device and resolved by SDS-polyacrylamide gel electrophoresis (PAGE) on 10% acrylamide gels running 2.5 cm into the separating gel. Proteins were visualized with either silver or colloidal Coomassie blue stain (Invitrogen), and the lanes were divided into three sections.

Excised acrylamide gel sections were cut into approximately 1-mm^3 pieces. Gel pieces were then subjected to a modified in-gel trypsin digestion procedure (47). Gel pieces were washed and dehydrated with acetonitrile for 10 min, followed by the removal of acetonitrile. Pieces were then completely dried in a Speed-Vac. Rehydration of the gel pieces was done with 50 mM ammonium bicarbonate solution containing 12.5 ng/μl modified sequencing-grade trypsin (Promega) at 4°C. After 45 min, excess trypsin solution was removed and replaced with 50 mM ammonium bicarbonate solution to just cover the gel pieces. Samples were then placed in a 37°C room overnight. Peptides were later extracted by removing the ammonium bicarbonate solution, followed by one wash with a solution containing 50% acetonitrile and 5% acetic acid. The extracts were dried in a Speed-Vac (~1 h) and then stored at 4°C until analysis. On the day of analysis, the samples were reconstituted in 5 to 10 μl of high-performance liquid chromatography solvent A (2.5% acetonitrile, 0.1% formic acid). A nanoscale reverse-phase high-performance liquid chromatography capillary column was created by packing 5-μm C_{18} spherical silica beads into a fused silica capillary (100-μm inner diameter by ~12-cm length) with a flame-drawn tip (41). After equilibrating the column, each sample was loaded onto the column via a Famos autosampler (LC Packings). A gradient was formed, and peptides were eluted with increasing concentrations of solvent B (97.5% acetonitrile, 0.1% formic acid). As each peptide was eluted, they were subjected to electrospray ionization and fed into an LTQ linear ion-trap mass spectrometer (ThermoFinnigan). Eluting peptides were detected, isolated, and fragmented to produce a tandem mass spectrum of specific fragment ions for each peptide. Peptide sequences (and, hence, protein identity) were determined by matching protein or translated nucleotide databases with the acquired fragmentation pattern by the software program SEQUEST (ThermoFinnigan) (17).

ZBP-89 antibody generation. Custom rabbit polyclonal antiserum was generated using a synthetic peptide corresponding to amino acids 1 to 14 of mouse ZBP-89 (MNI DDK LEG LFL KC) coupled to keyhole limpet hemocyanin (Sigma-Genosys). Protein A-purified immunoglobulin G (IgG) from the third bleed was used for experiments reported here and is designated "N14."

co-IP assays. For endogenous GATA-1 co-IP experiments, 3 to 5 mg of nuclear extract protein was treated with DNase I (1 μg/ml), RNase A (1 μg/ml), and ethidium bromide (50 μg/ml) and incubated with 25 to 50 μg of GATA-1 N6 (Santa Cruz) antibody on a rotating wheel at 4°C overnight. The next day, protein G/A-Sepharose beads (Sigma) were added, and the suspension was incubated for an additional 3 h at 4°C. The beads were washed four times in BC139K for 15 min and then heated at 95°C to 100°C in Laemmli SDS-PAGE buffer for 5 min. Eluted material was used for Western blot analysis. For interaction mapping studies, COS-7 cells were transiently cotransfected with 5 μg of plasmids expressing either FLAG- or V5-His-tagged protein constructs using FuGene 6 reagent (Roche) in 10-cm culture plates. Two days after transfection, nuclear extracts were prepared, immunoprecipitated with anti-FLAG M2 agarose beads (Sigma) as previously described (54), and processed for Western blot analysis.

Sephacryl S400 gel filtration chromatography. Crude nuclear extracts were prepared from uninduced L8057 cells as previously described (12) and dialyzed against 50 volumes of cold BC100 buffer (100 mM KCl, 12 mM NaCl, 0.8 M

$MgCl_2$, 20 mM Tris-HCl [pH 7.9], 0.2 mM EDTA, 20% [vol/vol] glycerol, 1 mM dithiothreitol, 0.2 mM phenylmethylsulfonyl fluoride, 0.1% protease inhibitor cocktail [Sigma]). The dialysate was centrifuged twice at 25,000 × *g* for 30 min at 4°C. The final supernatant (~15 mg of total protein) was injected into a 5-ml loop of a DuoFlow (Bio-Rad) fast protein liquid chromatography apparatus and run over a HiPrep Sephacryl S400 26/60 column (Amersham Pharmacia Biotech) in cold BC100 buffer at 0.5 ml/min with collection of 1-ml fractions. Molecular mass standards were aldolase (177 kDa), catalase (240 kDa), ferritin (438 kDa), and thyroglobulin (670 kDa).

Zebrafish morpholino experiments. Morpholino oligomers targeting the following zebrafish genes were synthesized by Gene Tools (Philomath, OR): *GATA-1* (5′-CTG CAA GTG TAG TAT TGA AGA TGT C-3′), *FOG-1* (5′-TCA TGT CCC CCT TAC CTC ACT GGC A-3′), *ZBP-89* (5′-ATA TTA AAC CTT TGC AGG C-3′), and ZBP-89 inverted sequence control (5′-CGG ACG TTT CCA AAT TAT A-3′). Morpholinos at the following working concentrations were microinjected into transgenic CD41-eGFP (32) fertilized zygotes at the one-cell stage: 3 mM zfp148, 3 mM zfp148 inverted control, 0.3 mM FOG-1, and 0.5 mM GATA-1. Injected embryos were analyzed for anemia by staining with *o*-dianisidine at 3 days postfertilization (dpf) and for presence of eGFP-positive cells at 4 dpf on a Nikon microscope equipped with a 10× objective (numerical aperture, 1.4). Fluorescence images were acquired with an Orca IIER charge-coupled-device camera (Hamamatsu). Electronic shutters and image acquisition were under the control of Metamorph software (Molecular Devices).

For reverse transcription (RT)-PCR analysis, injected embryos were harvested at ~4 dpf, and total RNA was isolated using the Qiagen RNA isolation kit. cDNA was synthesized using oligo(dT), and PCR was carried out with primers for *EF1*α, *GFP*, *CD41*, and c-*mpl*, as previously described (32), or forward primer 5′-CAT CAC AGC GAA AGG GTT TT-3′ and reverse primer 5′-CGC CTG CAA AGA TTC TCA CT-3′ for ZBP-89 using standard protocols. RT-PCR products were resolved on a 2% agarose gel and transferred onto nylon. Hybridization of the nylon membrane with ^{32}P-kinased internal 19-mer oligonucleotides for the respective genes was carried out using standard protocols. For ZBP-89 RT-PCR, [^{32}P]dCTP-incorporated PCR products were analyzed directly.

Generation of zbp89$^{gt/gt}$ ES cell line and characterization. The parental wild-type (WT) ES cell line E14tg2A and heterozygous ZBP-89 gene trap (GT) ES cell clone XB878 were obtained from BayGenomics. ZBP-89$^{wt/gt}$ ES cells were passaged on gelatin-treated plates and selected at high G418 concentrations (6 to 8 mg/ml) as previously described (36). G418-resistant clones were analyzed by Southern blotting using EcoRV digestion and probed with a 600-bp DNA fragment generated by PCR from E14tg2A genomic DNA using primers 5′-CAG GCA TCA GAG CTG TCT-3′ (forward) and 5′-GAA AGT CAC TGT GGA TCT GG-3′ (reverse), gel purified, and [^{32}P]dCTP labeled using a random primed labeling kit (Roche). For PCR genotyping, the WT allele was amplified by WT forward primer 5′-GCC CGT CAT AAT TTA GGT TGT GTA A-3′ and WT reverse primer 5′-AGT GTT GAC ATG ATG CCC TGA GTG A-3′. The GT allele was detected using the WT forward primer and a GT-specific reverse primer (5′-AGC GGA TCT CAA ACT CTC CTC CTT C-3′). Quantitative real-time PCR analysis of the GT allele from chimeric fetal liver was performed using β-galactosidase–neomycin phosphotransferase/LacZ primer sets (forward primer 5′-AAT CTC TAT CGT GCG GTG GT-3′ and reverse primer 5′-CAG CAG CAG CAG ACC ATT TT-3′) and normalized to β-actin DNA levels using forward primer 5′-TAA CAA TGG CTC GTG TGA CAA-3′ and reverse primer 5′-AAG TTC AGT GTG CTG GGA GTC T. Relative levels were determined and compared to those obtained from ZBP-89$^{gt/gt}$ ES cells, which were set at 100%. For transcript analysis, total RNA was isolated using a Qiagen RNeasy system, reverse transcribed with Superscript (Invitrogen), and amplified by PCR using the primer pairs 5′-ATT GAC GAC AAA CTG GAA GG-3′ (forward) and 5′-AGG CTT CTC TCC ACT GTG AG-3′ (reverse) for exons 4 to 9 and 5′-TTC TTT CTC AAC TCA ACA GC-3′ (forward) and 5′-TTA AGT GCA TAC TGC AGT CC-3′ (reverse) for exons 3 and 4.

In vitro differentiation of mouse ES and fetal liver cells. Mouse ES cells were differentiated in vitro into hematopoietic cells as previously described (59). ZBP-89 GT ES cells were maintained in 2 mg/ml of G418, and 2×10^4 cells were seeded into 5 ml of embryoid body generation medium containing 25 ng/ml interleukin-11 (IL-11) and 100 ng/ml stem cell factor (SCF). Embryoid bodies were harvested on day 7 and dissociated, and 4.5×10^5 cells were plated onto 3 ml of methyl cellulose medium containing 2 U/ml erythropoietin (EPO), 100 ng/ml SCF, and 5 ng/ml thrombopoietin (TPO) for erythroid differentiation and MegacultC (Stem Cell Technologies) medium containing 50 ng/ml TPO, 10 ng/ml IL-3, 20 ng/ml IL-6, and 50 ng/ml IL-11 for megakaryocyte differentiation. Colonies were scored after 9 days (erythroid) or 12 days (megakaryocyte). Fetal livers from E14.5 mouse embryos were harvested, processed into single-cell suspensions, and cultured in vitro using Methocult (Stem Cell Technologies) medium containing cytokines for BFU-E (50 ng/ml SCF, 10 ng/ml IL-3, 10 ng/ml IL-6, and 3 U/ml EPO) for 8 days or MegacultC (Stem Cell Technologies) medium with cytokines for CFU-MK (50 ng/ml TPO, 10 ng/ml IL-3, 20 ng/ml IL-6, and 50 ng/ml IL-11) for 10 days.

Retroviral infection. Vesicular stomatitis virus G-pseudotyped retroviral particles were generated via transient transfection of the stable packaging cell line 293 GPG with plasmid MMP-ZBP-89-IRES-Puro. ZBP-89$^{gt/gt}$ ES cells on gelatinized 96-well plates were incubated with concentrated retroviral supernatants at a multiplicity of infection of ~2 to 3 in ES medium containing 8 mg/ml polybrene for 1 h at 4°C followed by 4 h at 37°C in 5% CO_2. Cells were washed and incubated in ES medium for 2 days, followed by selection in 2 μg/ml puromycin on gelatinized plates.

Histology and cytology. Cytocentrifuge preparations were stained with May-Grunwald-Giemsa according to standard procedures. Acetylcholinesterase (AchE) staining was performed as previously described (27).

Generation and analysis of diploid/tetraploid chimeric mice. C57BL/6 blastocyst-stage embryos were injected with 6 to 10 ZBP-89 GT ES cells and transferred to pseudopregnant females for further development as previously described (19). For tetraploid complementation studies, 10 to 15 ZBP-89$^{gt/gt}$ ES cells were injected into tetraploid (4n) host blastocysts (14). Hemoglobin and glucose phosphate isomerase (GPI) analyses were performed as described previously (42, 43), and densitometric analysis was carried out using a GS-800 calibrated densitometer (Bio-Rad) and Quantity One software.

ChIP assay. ChIP was performed essentially as previously described (40). A total of 1×10^7 cells per IP were cross-linked at 5×10^5 cells/ml with 0.4% formaldehyde (final concentration) for 10 min at room temperature. Antibodies used were GATA-1 (N6; Santa Cruz), GATA-2 (H-116; Santa Cruz), and ZBP-89 (N14). DNA-protein-antibody complexes were eluted from Sepharose beads in 150 μl of elution buffer (1% SDS) at room temperature. For sequential IP, the beads were eluted in 80 μl followed by fivefold dilutions in IP dilution buffer (20 mM Tris-HCl, 2 mM EDTA, 150 mM NaCl, 1% Triton, 0.01% SDS) to reduce the SDS concentration to 0.2% before proceeding with second antibody IP. Results were quantified using real-time PCR with Sybr green dye on an iCycler system (Bio-Rad). A standard curve was generated from serial dilutions of input sample for each primer pair. All PCR signals from IP samples were referenced to their respective input standard curves.

PCR primer sequences used for ChIP are as follows: 5′-GGA GGG GAT ATG GGG TAA GAG ACT-3′ (forward) and 5′ CCA AGG CCA GCA AGA AGA CAT-3′ (reverse) for c-*mpl*, 5′-CAG GGA AGG TGA AAA GAA AAT AAG-3′ (forward) and 5′-TTG TAA TGC TGG TGT AAG TAA TGT-3′ (reverse) for β-*Globin* hypersensitive site 2 (HS2), 5′-TCC CTT ATC TAT GCC TTC CCA G-3′ (forward) and 5′-ATG AAG GGT GCC TCT AAG GAC A-3′ (reverse) for *GATA-1* HS1, and 5′-TGA TGG CTT CTA CTA GGC ACA CG-3′ (forward) and 5′-GGC TTC ACT CCC AGG AAT GTA GG 3′ (reverse) for *GATA-1* upstream. All primer pairs produced a single product based on melting-curve analysis.

All experiments involving mice and zebrafish were approved by the Animal Care and Use Committees at Children's Hospital Boston and Brigham and Women's Hospital.

RESULTS

Tandem affinity purification of GATA-1-containing complexes. In order to gain further insight into GATA-1 regulation during megakaryopoiesis, we purified GATA-1-containing multiprotein complexes from murine L8057 megakaryoblastic cells. These cells can be induced to differentiate by treatment with the phorbol diester TPA (26). To aid in the purification, we took advantage of a recently described technique for metabolic biotin tagging of recombinant proteins in mammalian cells (11). L8057 clones that stably express the *E. coli* biotin ligase *birA* alone or *birA* and recombinant GATA-1 containing a 23-amino-acid *birA* recognition motif fused to its N terminus were generated (Fig. 1A). We also included a FLAG epitope amino terminal to the biotin tag to allow for a tandem affinity purification procedure. Western blot analysis using anti-GATA-1 antibody revealed endogenous GATA-1 protein in nuclear extracts from both cell lines, as expected (Fig. 1B). In cells coexpressing *birA* and the GATA-1 fusion protein, a sec-

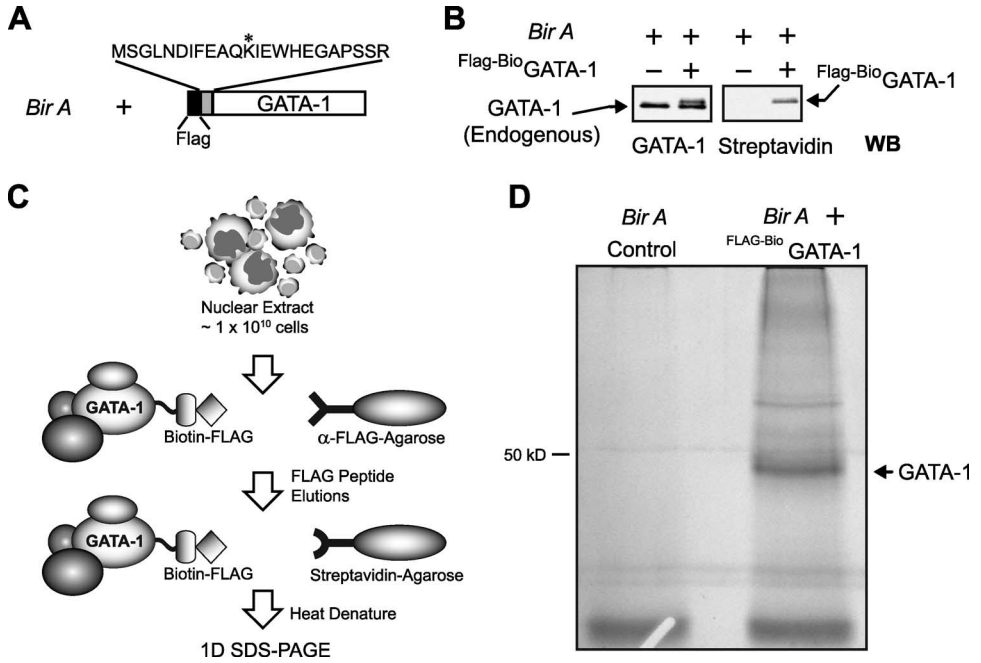

FIG. 1. Tandem affinity purification of $^{FLAG\text{-}Bio}$GATA-1 containing multiprotein complexes. (A) Schematic diagram of recombinant GATA-1 containing the amino-terminal FLAG peptide (black box) and the *birA* recognition sequence (gray box) ($^{FLAG\text{-}Bio}$GATA-1). The biotin acceptor lysine is indicated with an asterisk. BirA, *E. coli* biotin ligase. (B) Western blot (WB) analysis of nuclear extracts from L8057 clones stably expressing *birA* alone or *birA* and $^{FLAG\text{-}Bio}$GATA-1 probed with anti-GATA-1 antibody (left) or stripped and reprobed with streptavidin-horseradish peroxidase (right). (C) Schematic diagram of tandem anti-FLAG immunoaffinity and streptavidin affinity purification. (D) Representative silver-stained SDS-PAGE gel of copurified proteins. The expected position of GATA-1 is indicated by an arrow.

ond band with slightly slower mobility was observed, representing the larger, recombinant protein. Stripping and reprobing the blots with a streptavidin-horseradish peroxidase conjugate revealed a band corresponding to the recombinant GATA-1, demonstrating in vivo biotinylation. We purposefully chose a clone that expresses relatively low levels of recombinant GATA-1 (less than the endogenous protein level) to minimize potential perturbations that could arise from GATA-1 overexpression. Treatment of these cells with TPA showed no significant difference in maturation potential compared to that of parental cells, indicating the absence of a dominant negative effect of the tagged GATA-1 (data not shown).

Tandem anti-FLAG immunoaffinity and streptavidin affinity purification was performed on crude nuclear extracts from TPA-induced cells, and copurified proteins were separated by one-dimensional SDS-PAGE (Fig. 1C and D). Little detectable protein was observed in the control lane (*birA* alone) after silver staining. In contrast, an intense band corresponding to GATA-1 was present in the experimental lane, along with multiple additional bands. The entire lane was analyzed by microcapillary liquid chromatography/tandem mass spectrometry after in situ trypsinization, and proteins were identified using SEQUEST software. The results of five independent purifications are summarized in Table 1. As expected, GATA-1 and several previously established interacting proteins (and their associated factors) were identified. These include FOG-1 (54); the entire NuRD complex, which binds to FOG-1 (24, 45); SCL/TAL-1, Ldb1, and their interacting partners HTF4, SSBP-1/3, and SSBP-2/4 (13, 58, 63); Runx-1 and its heterodimeric partner CBF-β (16); Fli-1 (15); and SP1 (35).

ZBP-89 (zfp148/BERF-1/BFCOL1). In addition to the previously reported interacting proteins, we reproducibly isolated peptides corresponding to the ZBP-89 protein (also called zfp148, BERF-1, and BFCOl1) (see Fig. S1 in the supplemental material for peptide sequences). In separate experiments, we also recovered ZBP-89 in GATA-1 multiprotein complex purifications from induced MEL cells (Table 1). ZBP-89 is a ubiquitously expressed transcription factor that contains a cluster of four Krüppel-type zinc fingers, two basic domains, an acidic domain, and a predicted PEST (proline, glutamic acid, serine, and threonine) sequence (34) (Fig. 2A). Previous studies indicated that it binds with high affinity to GC-rich DNA sequences (proposed consensus sequence of CC [T/A]CCCCC) (2).

Validation of interaction between GATA-1 and ZBP-89. Western blot analysis of the anti-FLAG-streptavidin affinity-purified material using a previously established anti-ZBP-89 antibody (34) showed a band migrating at the expected position for ZBP-89 (~105 kDa) in the experimental lane but not in the control lane (Fig. 2B). We further validated the interaction between GATA-1 and ZBP-89 by IP experiments with endogenous proteins in L8057 and MEL cells (Fig. 2C) and recombinant proteins transiently expressed in COS-7 cells (Fig. 2F to I). The interaction appears to be via protein-protein contacts rather than through intervening DNA or RNA, since the co-IP assays shown in Fig. 2D and E were performed in the presence of 50 μg/ml of ethidium bromide (28), DNase, and RNase. In addition, a non-DNA-binding mutant of GATA-1 (GATA-1^{C261P}) (33) interacts with ZBP-89 in L8057 cells (Fig. 2E).

TABLE 1. Partial list of GATA-1-associated proteins identified by whole-lane mass spectrometry

Protein identity	No. of peptides obtained						
	L8057 cells						MEL cells in expt 1[b]
	Expt 1[a]	Expt 2[a]	Expt 3[a]	Expt 4[b]	Expt 5[b,c]	Total	
GATA-1	18	11	12	11	18	61	7
FOG-1	39	37	29	11		124	2
SCL complex							
SCL	7	7		1		12	
HTF4	5	6	3		2	13	
Ldb1	9	4	2			13	
SSDBP2	3	1	1	1		5	
SSDBP3		1				1	
SSDBP1	1					1	
NuRD complex							
MBD2	2	2				5	
MBD3	4	1		1		6	
Mi-2β	14	20	15	4		50	
P66α	3	18	8			7	
P66β	11	12	9	1		29	
HDAC1[d]	7	7	10	3		25	3
HDAC2	4	4	2	2		12	1
MTA1	10	16	10	1		41	
MTA2	12	24	10	1		49	
RbAp48[d]	8	9	9	3	4	23	1
RbAp46	2	4	4	3		11	
Runx-1	4	1	1	3		12	
Cbf-β	3					3	
Fli-1	2					2	
SP1		1				1	
ZBP-89	3	1		3	2	9	2
Total proteins[e]	81	64	42	155	33		87
Total specific proteins[f]	58	37	20	93	13		33

[a] Tandem anti-FLAG immunoaffinity and streptavidin affinity purification.
[b] Single streptavidin affinity purification.
[c] Only selected bands were examined (i.e., not whole-lane analysis).
[d] Peptides also found in controls.
[e] Total number of proteins identified in experiment (≥1 peptide).
[f] Total number of specific proteins identified (>1 peptide) in experiment (i.e., proteins not identified in any control [BirA alone] sample).

The interaction domains of GATA-1 and ZBP-89 were mapped using co-IP assays of epitope-tagged proteins transiently expressed in COS-7 cells (Fig. 2F to I). These studies identify the zinc finger domain of GATA-1 (amino acids 200 to 338) as the minimal region tested that is sufficient for the GATA-1 interaction with ZBP-89. Given the high degree of amino acid sequence homology within the zinc fingers of all GATA family members, we also tested interactions with full-length FLAG-tagged GATA-2 (Fig. 2G) and FLAG-tagged GATA-3 (data not shown) and found binding above background levels. Mapping studies of ZBP-89 show that a region (amino acids 304 to 793) outside of its zinc finger domain is necessary and sufficient for GATA-1 binding (Fig. 2H and I).

If ZBP-89 and GATA-1 exist in a stable complex, one would expect them to comigrate on gel filtration chromatography. As shown in Fig. 2J, ZBP-89 migrates as a major peak centered between the 440-kDa and 669-kDa markers, corresponding to a "shoulder" region of the GATA-1 elution pattern. This profile almost exactly mirrors that of FOG-1, consistent with the formation of a subcomplex involving ZBP-89, GATA-1, and FOG-1. Since the mapping studies indicate that ZBP-89 binds to the zinc finger region of GATA-1, which includes the FOG-1 binding domain, we tested whether ZBP-89 binds GATA-1 via FOG-1. In support of this, we were able to coimmunoprecipitate ZBP-89 and FLAG-tagged FOG-1 expressed in COS-7 cells, which do not express GATA-1 (Fig. 2G). On the other hand, a mutant GATA-1 molecule with impaired FOG-1 binding (GATA-1^{V205G}) (9) interacts with ZBP-89 in L8057 cells, despite the lack of detectable FOG-1 recovery in the same coimmunoprecipitated material (Fig. 2D and E). These data suggest that ZBP-89 may make independent contacts with both GATA-1 and FOG-1.

Functional analysis of ZBP-89 in hematopoietic development. Next, we performed morpholino-mediated gene knockdown experiments in zebrafish embryos to probe the functional significance of ZBP-89 in hematopoiesis. These assays utilized CD41-eGFP transgenic fish, which express eGFP within the

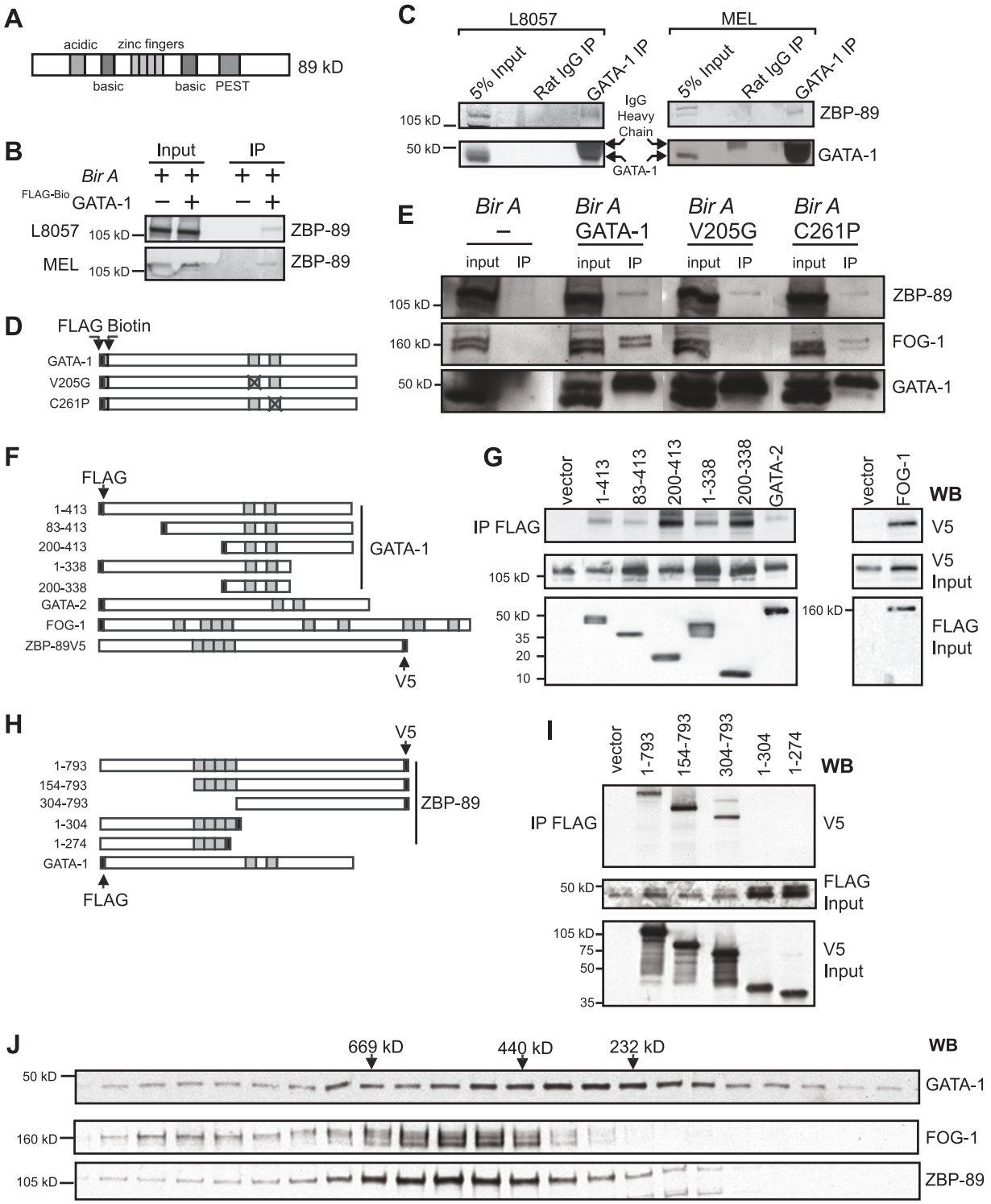

FIG. 2. Physical interaction between GATA-1 and ZBP-89. (A) Schematic diagram of ZBP-89 showing acidic, basic, zinc finger, and predicted PEST domains. (B) Western blot analysis using anti-ZBP-89 antibody (gift of Juanita Merchant) of input (5%) and eluates from anti-FLAG-streptavidin tandem affinity-purified material. (C) co-IP of endogenous GATA-1 and ZBP-89 from L8057 or MEL cells. IP was carried out using a rat IgG control or anti-GATA-1 antibody, and Western blotting was performed using anti-ZBP-89 antibody (N14). A band corresponding to the IgG heavy chain is indicated. (D) Schematic diagram of constructs used in panel E. (E) Western blot analysis of input (5%) or tandem affinity-purified (anti-FLAG followed by streptavidin) material from induced L8057 cells stably expressing *birA* alone or *birA* and $^{FLAG\text{-}Bio}$GATA-1, $^{FLAG\text{-}Bio}$GATA-1^{V205G}, or $^{FLAG\text{-}Bio}$GATA-1^{C261P} and probed with anti-ZBP-89, anti-FOG-1, or anti-GATA-1. Nuclear extracts were treated with DNase, RNase, and ethidium bromide. (F) Schematic diagram of constructs used in panel G. (G) Co-IP of ZBP-89^{V5} transiently coexpressed with ^{FLAG}Vector, ^{FLAG}GATA-1 truncation mutants, ^{FLAG}GATA-2, or ^{FLAG}FOG-1 in COS-7 cells. Nuclear extracts were immunoprecipitated with anti-FLAG antibody, and copurified proteins were analyzed by Western blotting (WB) with anti-V5 antibody.

thrombocyte lineage (equivalent to mammalian megakaryocytes and platelets) and more weakly in early multipotent hematopoietic progenitors (32). As shown in Fig. 3A, injection of a splice-site-directed ZBP-89 morpholino (panel c), but not an inverted sequence control (panel b), results in a marked reduction in the number of GFP-positive cells compared to those of uninjected animals (panel a). RT-PCR analysis of whole embryos confirms decreased mRNA levels of ZBP-89, eGFP, and CD41 compared to those of controls (Fig. 3B). In addition, levels of a second thrombocyte marker, c-*mpl*, were also reduced, suggesting a loss of the entire lineage rather than a specific effect on CD41 promoter activity. Importantly, morpholinos directed against FOG-1, but not GATA-1, phenocopy the loss of GFP-positive cells (Fig. 3A, d and e). Given the known compensatory FOG-1-dependent roles of GATA-1 and GATA-2 in early megakaryopoiesis (8), this suggests that ZBP-89 functionally interacts with FOG-1 and/or both GATA-1 and GATA-2.

As in mammals, erythroid development in zebrafish occurs in distinct waves, with an early primitive stage characterized by the expression of unique globin genes followed by a later definitive stage. The stage assessed in our morpholino experiments corresponds to primitive erythropoiesis. As shown in Fig. 3A, no significant difference in erythroid development, as assessed by staining for hemoglobinized cells with *o*-dianisidine (benzidine), was observed in the ZBP-89 morphants compared to controls (panels f to h). In contrast, morpholino knockdown of GATA-1 and FOG-1 results in markedly reduced benzidine staining (Fig. 3A, i and j). Thus, ZBP-89 is either dispensable for primitive erythropoiesis or functional at low levels.

Disruption of ZBP-89 in murine ES cells by GT insertion. We next examined the requirement for ZBP-89 in mammalian hematopoiesis using a murine GT ES clone available from BayGenomics (clone XB878). In this clone, the GT vector has inserted between exons 4 and 5 of the ZBP-89 locus (Fig. 4A). This is predicted to generate a fusion protein consisting of the first 111 amino acids of ZBP-89 linked to the β-galactosidase–neomycin phosphotransferase marker gene. Eighty-six percent of the full-length ZBP-89 coding sequence would be lost, including all four zinc fingers. We confirmed the insertion site by 5′ rapid amplification of cDNA ends (data not shown) and Southern blot analysis (Fig. 4B) and generated homozygous ZBP-89 GT (ZBP-89$^{gt/gt}$) ES cell clones by selection in high G418 concentrations (Fig. 4B). RT-PCR analysis using primers specific for full-length ZBP-89 mRNA transcripts (exons 4 to 9) shows about a 50% reduction of levels in heterozygous cells compared to those of the WT and barely detectable levels in homozygous cells (Fig. 4C). The small amount of residual WT transcripts may be due to low-level splicing around the GT vector. Lastly, we generated "rescued" cells by retrovirally expressing ZBP-89 in the ZBP-89$^{gt/gt}$ ES cells. Western blot analysis using a polyclonal antibody raised against an amino-terminal epitope (amino acids 1 to 14) shows a nearly complete loss of the ZBP-89 protein in ZBP-89$^{gt/gt}$ cells and nearly WT levels in the retrovirally rescued cells (Fig. 4D). Heterozygous cells have ZBP-89 levels similar to those of WT ES cells (see Discussion). As expected, our antibody detected increasing levels of the ZBP-89–β-galactosidase–neomycin phosphotransferase GT fusion product ("gt-zbp89," with a predicted molecular mass of ~160 kDa) in the ZBP-89$^{gt/+}$ and ZBP-89$^{gt/gt}$ cells, respectively.

In vitro differentiation of ZBP-89$^{gt/gt}$ ES cells. Two-step in vitro differentiation of the ES cells was performed to examine the requirement for ZBP-89 during definitive hematopoiesis. As shown in Fig. 4E and F, there is a marked reduction of visibly hemoglobinized colonies from the ZBP-89$^{gt/gt}$ ES cells compared to those of the WT, despite plating equal numbers of cells. Cytospin and May-Grunwald-Giemsa stainings show mature erythroid forms in the WT cultures but cells that appeared to be blocked at a stage similar to that reported for GATA-1 and FOG-1 deficiency (53, 59) in the ZBP-89$^{gt/gt}$ ES-derived cultures (Fig 4E, d and e, black arrows). Under megakaryocyte growth conditions, we observed a marked reduction in megakaryocyte colony formation, as detected by histochemical staining for AchE, a marker of murine megakaryocytes (Fig. 4E, g and h). Importantly, the retroviral expression of ZBP-89 rescues both erythroid and megakaryocyte developmental blocks, ruling out a defect unrelated to the ZBP-89 loss in the GT ES cells (Fig. 4E, c, f, and i, and F). We conclude that ZBP-89 is required for definitive erythropoiesis and megakaryopoiesis in vitro.

Requirement for ZBP-89 in vivo. ZBP-89 GT mice were generated to examine the requirement of ZBP-89 in vivo. No significant differences in growth, fertility, or hematologic indices were apparent in heterozygous animals compared to WT littermates (data not shown). However, we failed to recover any live-born homozygous GT animals among 35 offspring of heterozygous parent matings, consistent with an embryonic lethal phenotype (see Table S1 in the supplemental material). We next examined embryos of different gestational ages. At E8.5, homozygous animals were recovered and phenotypically indistinguishable from heterozygous and WT animals. However, by E10.5, all homozygotes were dead, as defined by the lack of a heartbeat at the time of dissection (Fig. 5A). Although some variability in phenotype was observed, all homozygotes were significantly growth retarded and markedly pale and contained an open neural tube. Yolk sac vasculature was disorganized in some cases and either lacked visible red blood cells or contained small pools of primitive erythrocytes. Only dead, resorbing homozygous embryos were observed at E12.5, and none were recovered at E16.5. Taken together, these data indicate that the loss of ZBP-89 results in embryonic lethality between E8.5 and E10.5.

Inputs (5%) are shown. (H) Schematic diagram of constructs used in panel I. (I) co-IP of ZBP-89^{V5} truncation mutants transiently coexpressed with ^{FLAG}GATA-1 in COS-7 cells. Nuclear extracts were immunoprecipitated using anti-FLAG antibody, and copurified proteins were analyzed by Western blotting with anti-V5 antibody. Inputs (5%) are shown. (J) Sepharcryl-S400 gel filtration chromatography of nuclear extracts from uninduced L8057 cells. Western blot analysis with anti-GATA-1, anti-FOG-1, or anti-ZBP-89 antibodies of every fifth fraction is shown. Elution positions of molecular mass standards are indicated.

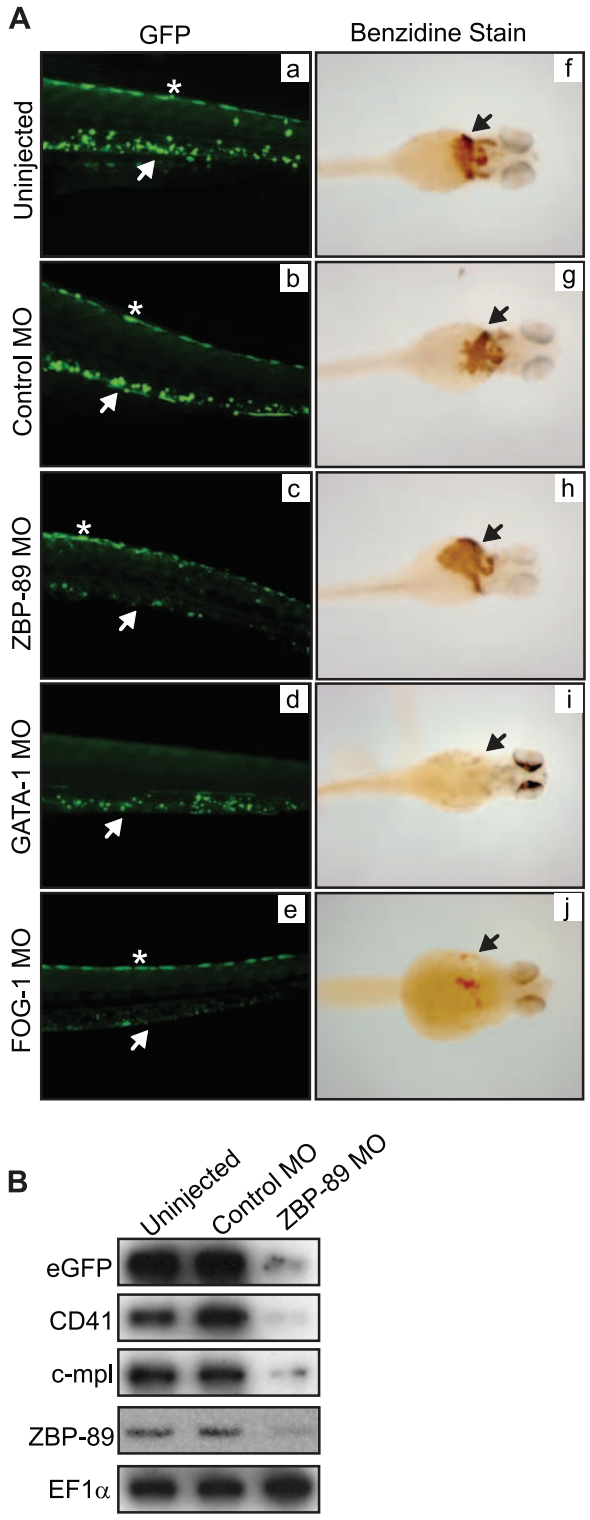

FIG. 3. Transient knockdown of ZBP-89 expression in CD41-eGFP transgenic zebrafish embryos (A, a to e) Fluorescent microscopy images of uninjected CD41-eGFP transgenic zebrafish embryos at 4 dpf or those injected at the one-cell stage with ZBP-89 control (inverted sequence), ZBP-89, GATA-1, or FOG-1 antisense morpholinos (MO). The white arrows indicate GFP-positive thrombocytes. The asterisks show autofluorescent chromatophore pigment cells along the dorsum of some fish. (f to j) *o*-Dianisidine (benzidine) stains of zebrafish embryos injected at the one-cell stage with the indicated morpholinos and examined at 3 dpf. Positive cells are brown/red (black arrows). (B) RT-PCR analysis for eGFP, CD41, c-*mpl*, ZBP-89, and EF1α expression in 4-dpf CD41-eGFP transgenic embryos either uninjected or injected with control or ZBP-89 morpholinos. A Southern blot of PCR products is shown, except for ZBP-89, which represents the [^{32}P]dCTP-incorporated PCR product.

Tetraploid complementation analysis. Many of the defects present in the ZBP-89$^{gt/gt}$ embryos resemble those due to placental insufficiency. In order to test this, tetraploid complementation experiments were carried out. In 6 out of 10 animals generated by this method, we observed live embryos at E9.5 to E10.5 that were well grown and hemoglobinized and that contained grossly normal vasculature and closed neural tubes (Fig. 5B). In these cases, the entire embryo proper was derived from the ZBP-89$^{gt/gt}$ ES cells based on LacZ staining and RT-PCR analysis. These results indicate that the early gross developmental defects of ZBP-89$^{gt/gt}$ embryos are most likely due to deficiencies in placental function. Consistent with this, immunohistochemical analysis of WT placenta showed robust ZBP-89 expression (see Fig. S3 in the supplemental material). Recovery of abundant, normal-appearing erythrocytes from E10.5 tetraploid complementation embryos provides further evidence that ZBP-89 is dispensable for primitive erythropoiesis (Fig. 5B). Despite the fact we could rescue some of the early lethality phenotype, we did not observe any live embryos by E12.5 to E13.5 (data not shown). This may be due to other abnormalities in the embryo, and this limits our ability to use tetraploid complementation to assess ZBP-89's role during definitive hematopoiesis.

Analysis of ZBP-89$^{gt/gt}$ chimeric mice. We therefore turned to chimeric mouse analysis. Cells derived from the GT ES cells can be selected using G418 since they express a neomycin resistance gene. In the first set of studies, we pooled E14.5 fetal liver cells from nine chimeric embryos. Allele-specific PCR and quantitative real-time PCR for LacZ DNA indicated an average of ~25% ZBP-89$^{gt/gt}$-derived cells in this preparation (Fig. 5C). Control "chimeric" animals were derived using WT donor ES cells. Fetal liver cells from the control animals generated large, well-hemoglobinized colonies with mature erythroid cells after culture for 8 days in semisolid medium with EPO, IL-3, IL-6, and SCF in the absence of G418 (Fig. 5D and E). As expected, the inclusion of ≥1 mg/ml G418 resulted in a nearly complete loss of colony formation. In contrast, numerous colonies grew from the ZBP-89$^{gt/gt}$ chimeric fetal liver preparations in the presence of 1 or 2 mg/ml G418, representing exclusively ZBP-89$^{gt/gt}$-derived cells. The total number of colonies was 29% ± 5.9% (n = 3) and 32% ± 3.2% (n = 3) of those generated in the absence of G418, respectively. This is close to the expected frequency of ZBP-89$^{gt/gt}$-derived cells in the starting population based on the quantitative LacZ PCR analysis (~25%). If ZBP-89 were dispensable for erythroid maturation, we would therefore expect about 30% of the number of hemoglobinized colonies in the presence of ≥1 mg/ml G418 compared to those grown in its absence. However, we observed fewer (16% ± 1.2% at 1 mg/ml [n = 3] and 17% ± 5.3% at 2 mg/ml [n = 3]; $P < 0.01$), consistent with impaired erythroid development. Cytospin and May-Grunwald-Giemsa

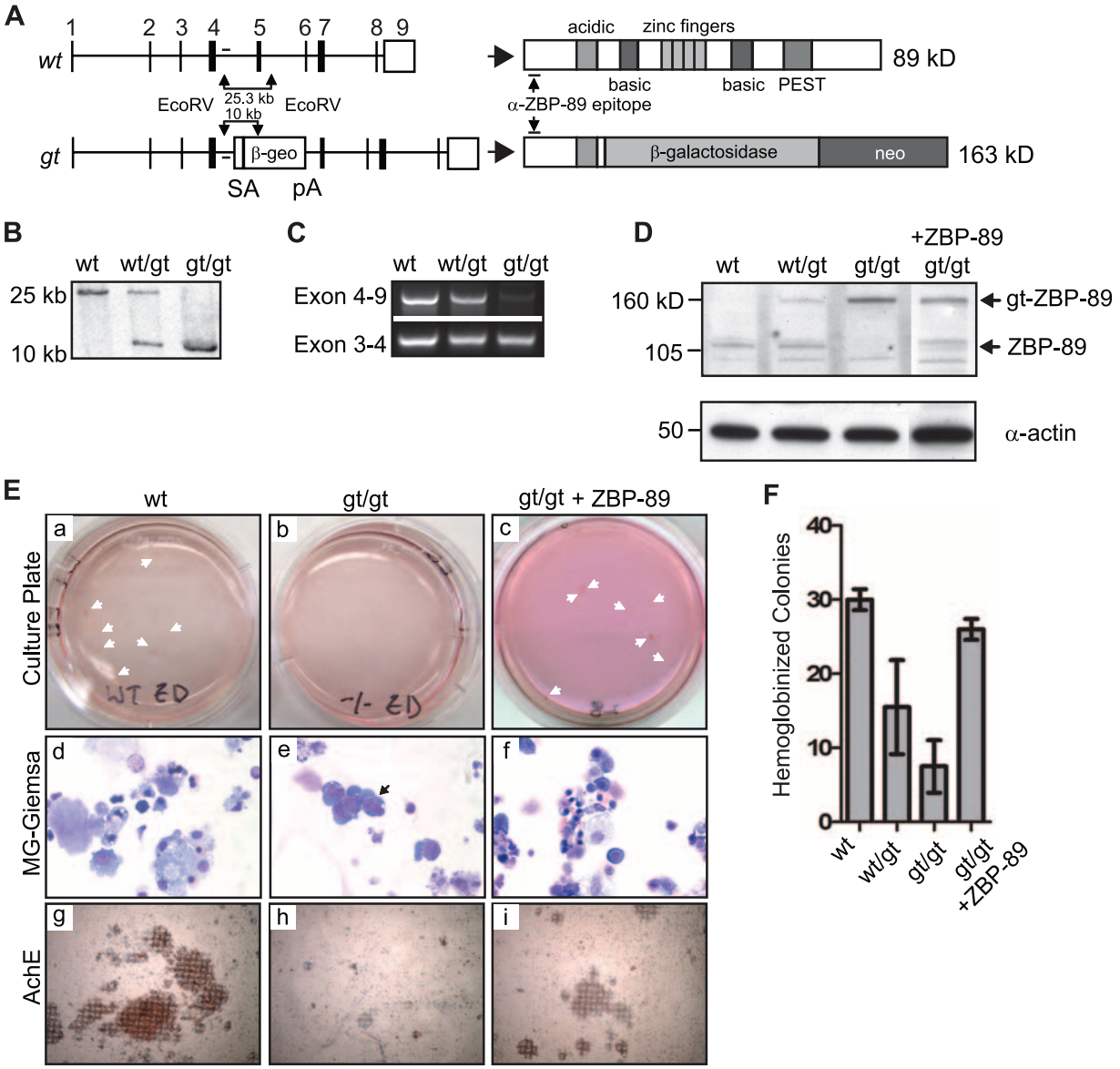

FIG. 4. In vitro differentiation of ZBP-89 GT ES cells. (A, left) Schematic representation showing the GT vector insertion site within the ZBP-89 locus. SA, splice acceptor site; β-geo, β-galactosidase–neomycin phosphotransferase; PA, polyadenylation sequence. Positions of EcoRV restriction sites and the probe used for Southern blot analysis in B are indicated as arrows and a horizontal bar, respectively. (Right) Predicted protein products generated from WT and GT alleles. (B) Southern blot analysis of WT, ZBP-89$^{gt/+}$, and ZBP-89$^{gt/gt}$ ES cell genomic DNA digested with EcoRV and hybridized with the probe shown in panel A. (C) RT-PCR analysis of WT, ZBP-89$^{gt/+}$, and ZBP-89$^{gt/gt}$ ES cells using primer sets that detect full-length ZBP-89 mRNA transcripts only (top) or both full-length and GT mRNA transcripts (bottom). (D) Western blot analysis of nuclear extracts from WT, ZBP-89$^{gt/+}$ and ZBP-89$^{gt/gt}$ ES cells, and ZBP-89$^{gt/gt}$ ES cells retrovirally expressing ZBP-89 using anti-ZBP-89 (N14) (top) or antiactin (bottom) antibodies. Expected migration positions of endogenous ZBP-89 and the ZBP-89–GT fusion product (gt-ZBP-89) are indicated. (E) Two-step in vitro differentiation of WT parental ES cells, ZBP-89$^{gt/gt}$ ES cells (gt/gt), or ZBP-89$^{gt/gt}$ ES cells retrovirally expressing ZBP-89 (gt/gt + ZBP-89). (a to f) Secondary plating carried out under definitive erythropoiesis conditions (EPO, SCF, and TPO for 9 days). (a to c) Photographs of representative culture dishes. Macroscopically visible red colonies are indicated by white arrows. (d to f) May-Grunwald-Giemsa stains of pooled cytospun cells. The black arrow indicates proerythroblast-like cells. (g to i) Secondary plating carried out under megakaryocytic growth conditions (MegacultC with TPO, IL-3, IL-6, and IL-11 for 12 days) and stained for AchE activity (orange/brown). Cells are counterstained with Harris' hematoxylin (blue). (F) Quantitation of red (hemoglobinized) colonies observed after erythroid in vitro differentiation for each of the genotypes. Equal numbers of starting cells (4.5×10^5 cells) were plated. Counts are displayed as the means of three cultures ± standard errors of the means.

staining of the residual cells shows many mast cells and some early erythroid forms (Fig. 5D). Likewise, there was poor megakaryocyte colony formation (AchE-positive cells) in the ZBP-89$^{gt/gt}$ chimeric fetal liver cell preparation incubated in the presence of G418 compared to cultures without G418, consistent with a requirement for ZBP-89 in fetal liver megakaryocyte development (Fig. 5F).

We also examined the contribution of ZBP-89$^{gt/gt}$ ES cells to

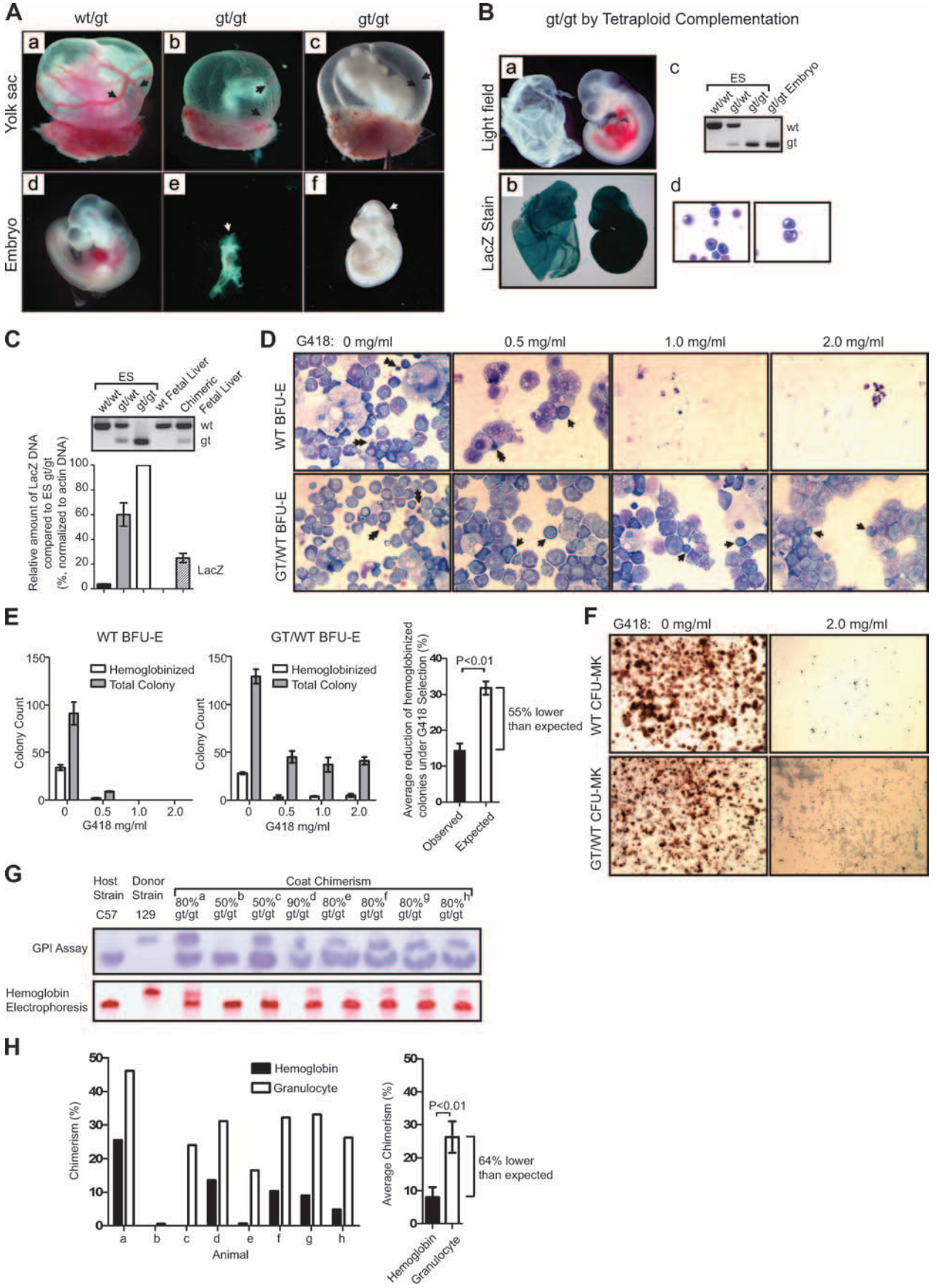
A
wt/gt
gt/gt
gt/gt
Yolk sac
Embryo
B
gt/gt by Tetraploid Complementation
Light field
LacZ Stain
ES
wt/wt
gt/wt
gt/gt
gt/gt Embryo
wt
gt
C
ES
wt/wt
gt/wt
gt/gt
wt Fetal Liver
Chimeric Fetal Liver
wt
gt
Relative amount of LacZ DNA compared to ES gt/gt (%, normalized to actin DNA)
LacZ
D
G418: 0 mg/ml
0.5 mg/ml
1.0 mg/ml
2.0 mg/ml
WT BFU-E
GT/WT BFU-E
E
WT BFU-E
GT/WT BFU-E
Hemoglobinized
Total Colony
Colony Count
G418 mg/ml
Average reduction of hemoglobinized colonies under G418 Selection (%)
P<0.01
55% lower than expected
Observed
Expected
F
G418: 0 mg/ml
2.0 mg/ml
WT CFU-MK
GT/WT CFU-MK
G
Host Strain
Donor Strain
Coat Chimerism
C57
129
80%a gt/gt
50%b gt/gt
50%c gt/gt
90%d gt/gt
80%e gt/gt
80%f gt/gt
80%g gt/gt
80%h gt/gt
GPI Assay
Hemoglobin Electrophoresis
H
Hemoglobin
Granulocyte
Chimerism (%)
Animal
Average Chimerism (%)
P<0.01
64% lower than expected
Hemoglobin
Granulocyte

circulating erythrocytes in adult chimeric mice. In this case, cells derived from the donor GT ES and WT host cells can be distinguished based on strain differences in hemoglobin isoforms, which migrate differently by electrophoresis. Although coat color can be used as a gauge of chimerism, we determined the level of bone marrow chimerism by measuring the relative abundance of strain-specific isoforms of the enzyme GPI from peripheral blood granulocytes. As shown in Fig. 5G and H, eight chimeric animals showed a significantly reduced contribution to hemoglobin levels from the ZBP-89$^{gt/gt}$ donor cells compared to what would be expected based on GPI isoform analysis (average of 64% lower than expected; $P < 0.01$). We conclude that ZBP-89 plays a functional role in definitive erythroid and megakaryocyte development in vivo.

Occupancy of gene regulatory elements by both ZBP-89 and GATA-1. Lastly, we examined several candidate GATA-1 genomic binding sites for ZBP-89 occupancy by ChIP assays. As shown in Fig. 6A, significant enrichment for both GATA-1 and ZBP-89 was observed at an enhancer element upstream of the GATA-1 gene itself (GATA-1 HS1) in induced L8057 and MEL cells. This region is located ~3.5 kb upstream of the hematopoietic-specific transcriptional start site (IE) and contains a functionally important GATA consensus binding site, an E-box element, and several phylogenetically conserved consensus ZBP-89 binding sequences located −56, +74, and +90 bp away from the GATA binding site (57). Control ChIP assays examining a region ~2 kb upstream, which lacks GATA and ZBP-89 consensus binding sequences, show only backgrounds levels of PCR amplification. Sequential ChIP assays in which chromatin fragments were first immunoprecipitated with anti-ZBP-89 antibody and the eluted material was then immunoprecipitated with anti-GATA-1 antibody (or vice versa) demonstrate simultaneous cooccupancy of this element by ZBP-89 and GATA-1 (Fig. 6B). ZBP-89 and GATA-1 chromatin occupancy was also detected at DNase I HS2 of the murine β-globin locus control region in induced MEL cells and the c-*mpl* promoter in induced L8057 cells (Fig. 6C).

In order to provide mechanistic information on how ZBP-89 and GATA-1 might cooperate in hematopoietic differentiation, we examined ZBP-89 occupancy at GATA-1 HS1 in G1E cells, a genetically engineered GATA-1$^-$ murine erythroid cell line that is arrested at a proerythroblast-like stage (60). As shown in Fig. 6D, significant enrichment for ZBP-89 was observed even in the absence of GATA-1. However, we cannot exclude GATA factor-independent binding since GATA-2 is present at this site in these cells. These results also show that ZBP-89 chromatin occupancy occurs at early stages of erythroid development, at least at the locus examined. Genetic complementation of these cells with an inducible form of GATA-1 shows relatively stable ZBP-89 occupancy at GATA-1 HS1 as GATA-1 binding occurs and the cells mature (see Fig. S4 in the supplemental material).

DISCUSSION

In this study, we identify the Krüppel-type zinc finger transcription factor ZBP-89 as being a novel component of GATA-1–FOG-1 multiprotein complexes and show that it plays a functional stage-specific role in erythroid and early megakaryocyte development in vivo. Moreover, we show the cooccupancy of ZBP-89 and GATA-1 at key *cis*-regulatory regulatory elements of certain erythroid cell- and megakaryocyte-specific genes in hematopoietic cells. These findings indicate a possible role for ZBP-89 in determining GATA factor binding site selectivity in vivo through the formation of multiprotein complexes with extended DNA binding specificity and affinity (Fig. 6E). Stabilization of such a complex by FOG-1, as our data suggest, could explain FOG-1's previously observed role in the context-dependent facilitation of GATA factor occupancy.

Potential role of ZBP-89 in globin gene regulation. In humans, the different β-globin-like genes are located in a cluster on chromosome 11 arranged in the order of their developmental expression. Key *cis*-acting DNA regulatory elements within an upstream locus control region and the globin gene-proximal promoters that are required for high-level and developmentally appropriate globin gene expression have been identified. These contain ~250-bp core regions that include clusters of binding sites for three major regulatory proteins: GATA, NF-E2, and "CACCC"-interacting factors. A variety of proteins have been shown to bind "CACCC"-type motifs, including SP1

FIG. 5. Analysis of ZBP-89 GT mice. (A) Photographs of representative E10.5 ZBP-89$^{wt/gt}$ and ZBP-89$^{gt/gt}$ murine embryos. (a to c) Embryos with yolk sac in place. (d to f) Embryos without yolk sac. Black arrows indicate yolk sac blood vessels. White arrows show open neural tubes (see Fig. S2 in the supplemental material for additional images). (B) Tetraploid complementation analysis. (a) Photograph of a representative E10.5 ZBP-89$^{gt/gt}$ embryo generated by tetraploid complementation. (b) LacZ staining of embryo and yolk sac. (c) Allele-specific genomic PCR from control ES cells or tetraploid complementation embryo proper (gt/gt). Positions of WT and GT products are indicated. (d) May-Grunwald-Giemsa stains of yolk sac blood. (C to F) ZBP-89$^{gt/gt}$/WT (diploid) chimeric embryo analysis. (C, top) Conventional PCR of WT and GT alleles showing the relative contribution of ZBP-89$^{gt/gt}$ cells in pooled E14.5 fetal liver cells used in panels D to F. Note that there is lower PCR efficiency for the GT allele, as indicated by the analysis of ZBP-89$^{gt/wt}$ ES cells. (Bottom) Quantitative real-time PCR analysis of samples shown in the top panel using primers specific to the GT LacZ gene. Levels are displayed relative to those obtained from ZBP-89$^{gt/gt}$ ES cells (set at 100% GT cells) after normalization to genomic β-actin DNA levels. (D) May-Grunwald-Giemsa stains of BFU-E colonies from WT or chimeric (GT/WT) E14.5 fetal livers cultured in 0, 0.5, 1.0, or 2.0 mg/ml G418. Double arrows indicate mature erythroid cells, and single arrows show immature erythroid precursors. (E) Number of total (gray bars) and red (hemoglobinized) (white bars) colonies from fetal liver cultures presented in panel D and graph showing expected (if ZBP-89 were dispensable) versus observed data. Cultures were performed in triplicate and are displayed as the means ± standard errors of the means. (F) AchE stains of CFU-Mk from WT or pooled chimeric (GT/WT) E14.5 fetal liver cells cultured in the absence or presence of 2 mg/ml G418. Cells are counterstained with Harris' hematoxylin. (G to H) Adult chimeric mouse analysis. (G) Peripheral blood granulocyte GPI electrophoresis (top) and matched peripheral erythrocyte hemoglobin electrophoresis from eight adult chimeric mice (a to h). The estimated percent donor chimerism based on coat color is indicated. (H, left) Densitometric analysis of data in panel G showing percent chimerism based on granulocyte GPI isoform versus erythrocyte hemoglobin isoform abundances. (Right) Graph showing means of the eight animals ± standard errors of the means, with difference in expected (based on GPI isoform abundance) and observed (based on hemoglobin isoform abundance) data indicated.

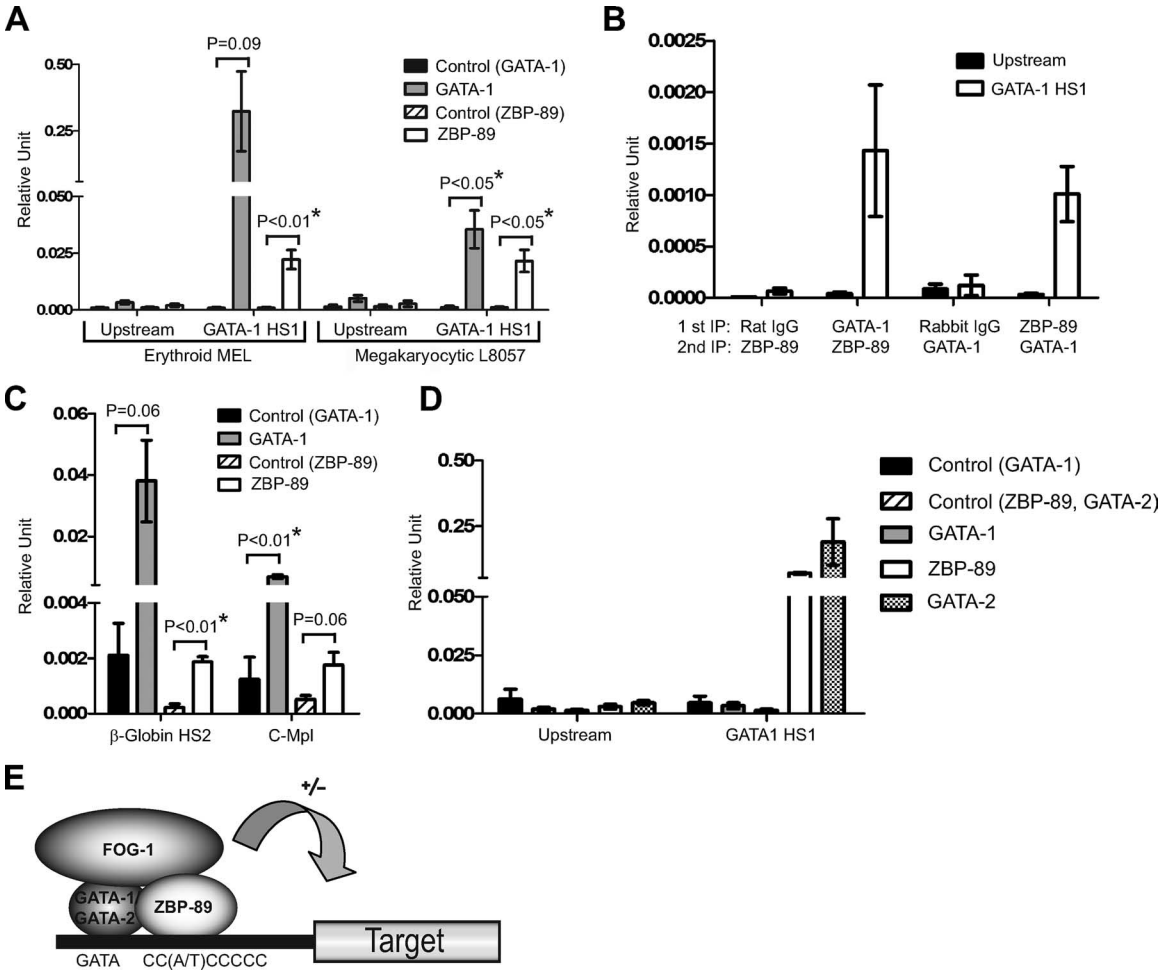

FIG. 6. Chromatin occupancy by ZBP-89 and GATA-1. (A) Quantitative real-time PCR ChIP analysis of ZBP-89 and GATA-1 chromatin occupancy at GATA-1 HS1 (57) in induced MEL and L8057 cells. Control antibodies are rat IgG for GATA-1 and preimmune IgG for ZBP-89. "Upstream" refers to the site ~2 kb 5′ to GATA-1 HS1, which is devoid of consensus GATA and ZBP-89 binding sites. PCR signals are related to a standard curve of input chromatin and are displayed as relative units. Asterisks indicate statistically significant differences ($P \leq 0.05$). (B) Sequential ChIP of ZBP-89 and GATA-1 at GATA-1 HS1 in induced MEL cells. Antibodies used for the first and second IP steps are indicated. Rabbit IgG refers to ZBP-89 preimmune IgG. (C) ChIP assays for GATA-1 and ZBP-89 at murine β-globin locus HS2 in induced MEL cells and the c-*mpl* promoter in induced L8057 cells. (D) ChIP assays for GATA-1, ZBP-89, and GATA-2 at GATA-1 HS1, or the upstream control region, in G1E cells. (E) Model of the cooperative DNA binding multiprotein complex involving GATA-1 or GATA-2, FOG-1, and ZBP-89.

and members of the X-KLF family, such as erythroid Krüppel-like factor (EKLF). However, the full complement of proteins that bind these elements in vivo is unknown. Li and colleagues previously characterized a "CACCC" box in the proximal promoter of the human γ-globin gene and showed that it is required for γ-globin gene expression during definitive, but not primitive, stages of erythropoiesis in transgenic mice (31). However, the responsible transactivating factor(s) has yet to be identified. The "CACCC" motif comprises the core ZBP-89 consensus binding site. Our data showing ZBP-89 chromatin occupancy of the murine β-globin HS2 region, its physical association with GATA-1, and its stage-specific requirement during definitive but not primitive erythropoiesis suggest that it may be another "CACCC" binding protein involved in globin gene regulation.

Two other recent reports support the hypothesis of a role for ZBP-89 in globin gene regulation. Brand and colleagues isolated multiprotein complexes involving the NF-E2 p45 heterodimeric partner MafK in uninduced and induced MEL cells and identified components using a quantitative proteomic technique (3). They found that in uninduced cells, MafK associates predominantly with the transcriptional repressor Bach1, the cofactor HET/SAF-B, and the NuRD and SWI/SNF complexes. However, in induced cells, MafK preferentially associates with NF-E2 p45, ZBP-89, SP2 and/or SP4, Ldb-1, p75, and the TIP coactivator complex. In fact, the relative enrichment for ZBP-89 in induced versus uninduced MEL cells is about an order of magnitude greater than that for any other component. Vernimmen and colleagues examined ZBP-89 binding in the murine α-globin locus in MEL cells and found high-level occupancy at HS8 and low-level occupancy at the proximal promoter (55).

Interplay between GATA-1, ZBP-89, and SP/X-KLF family proteins. In addition to the globin genes, the codistribution of functionally important "CACCC" motifs and GATA binding sites has been observed in *cis*-regulatory elements of a large

array of erythroid cell-specific genes, including erythroid pyruvate kinase; glycophorins A, B, C, and E; erythropoietin receptor; porphobilinogen deaminase; glutathione peroxidase; and GATA-1 (20, 57). Functionally codistributed GATA and GC-rich (SP1-type) binding sites have also been identified in *cis*-regulatory elements of megakaryocyte-specific genes such as αIIb, glycoprotein VI, and c-*mpl*. Both EKLF and SP1 physically interact and synergize with GATA-1 in transcriptional reporter assays (35). ZBP-89 has also been reported to heterodimerize with SP1 (64). Therefore, a complex interplay between ZBP-89, other members of the SP/X-KLF family, and GATA factors during erythroid and megakaryocytic differentiation may exist.

Potential role of ZBP-89 in GATA-1 gene regulation. Guyot and colleagues also examined ZBP-89 chromatin occupancy at GATA-1 HS1 (22). As we found, they detected significant ZBP-89 enrichment at this site as well as at the GATA-1 proximal promoter (IE) and a +3.5-kb enhancer element in L8057 cells. These findings suggest that ZBP-89 may play a direct role in regulating GATA-1 expression levels.

ZBP-89 mechanisms of action. Like many transcription factors, ZBP-89 can act either as a transcriptional activator or as a repressor depending on promoter and cell type context. Proposed mechanisms for its repressive function include antagonism of the potent transcriptional activator SP1 (64) and recruitment of histone deacetylases (62). In terms of activation, ZBP-89 has been shown to interact with the transcriptional coactivator p300 (1). Our kinetic data, along with the findings of Vernimmen et al. (55), indicate that ZBP-89 occupies chromatin at relatively early stages of erythroid maturation. Recruitment of p300 by ZBP-89 may therefore facilitate the "opening" of the local chromatin structure during differentiation, allowing access to additional factors.

Essential roles of ZBP-89 in vivo. Although our loss-of-function studies show a clear role for ZBP-89 in definitive erythroid and megakaryocytic development, we did observe the production of small numbers of mature cells. The presence of low levels of residual ZBP-89 in our experimental systems and/or a potential overlapping functional role of ZBP-99, a widely expressed ZBP-89 family member that binds similar DNA sequences in vitro (29), could account for an incomplete phenotype.

Takeuchi and colleagues reported previously that heterozygosity with respect to ZBP-89 results in infertility due to a defect in primordial germ cell development (49). It was therefore surprising that we easily obtained germ line transmission of the heterozygous ZBP-89 GT allele. Possible explanations for this discrepancy include (i) a dominant negative effect of the allele created by Takeuchi and colleagues, which is predicted to generate a carboxyl-truncated ZBP-89 molecule retaining the first three, and part of the fourth, zinc fingers and (ii) rescue of the germ cell defect by low levels of residual ZBP-89 in our experiments. The generation of additional gene-targeted alleles should help distinguish these possibilities.

Posttranslational regulation of ZBP-89 levels. ZBP-89 is predicted to contain a PEST domain. Such motifs target proteins for rapid proteolytic degradation and are often contained in highly regulated proteins (44). Several observations suggest that ZBP-89 protein levels may be regulated by posttranslational mechanisms, likely mediated through its PEST domain. First, ZBP-89$^{gt/+}$ ES cells have the same ZBP-89 protein level as WT ES cells despite having ~50% of their mRNA levels (Fig. 4). Second, retroviral expression of ZBP-89 in the ZBP-89$^{gt/gt}$ ES cells results in protein levels identical to those of WT ES cells, which seems unlikely unless a regulatory mechanism was placing a limit on steady-state protein levels. Third, the overexpression of ZBP-89 appears to be quite toxic in hematopoietic cell lines and primary cells (T. Moran and A. B. Cantor, unpublished observation). Fourth, the deletion of a carboxyl-terminal portion of ZBP-89, which includes the predicted PEST domain, results in about a 10-fold increase in protein levels when expressed in 293T cells compared to full-length ZBP-89, despite equivalent mRNA levels (Y. Schindler and A. B. Cantor, unpublished observation). Thus, mechanisms that modulate putative PEST-mediated protein decay may play important roles in regulating ZBP-89 activity and, consequently, its effects on hematopoietic differentiation.

ACKNOWLEDGMENTS

We thank Juanita Merchant for providing ZBP-89 antibody and rat ZBP-89 cDNA, Robert Handin for CD41-eGFP transgenic fish, Sung-Yun Pai for the FLAG-GATA-3 construct, and Stuart Orkin for G1E and G1-ER cells. We also acknowledge Ross Tomaino and Steven Gygi at the Taplin Mass Spectrometry Core Facility at Harvard Medical School for assistance with mass spectrometry.

This work was supported by grants from the NIH (R01 HL 075705 to A.B.C. and R01 DK070838 to B.H.P.), the American Society of Hematology (Junior Faculty Award to A.B.C.), and the March of Dimes (5-FY04-21, 1-FY06-365 to B.H.P.).

ADDENDUM IN PROOF

After acceptance of our study, we realized that we failed to reference the work of Li et al. (X. Li, J. W. Xiong, C. S. Shelley, H. Park, and M. A. Arnaout, Development **133:**3641–3650, 2006). This group performed zebrafish morpholino knockdown experiments and murine ES cell overexpression studies to demonstrate a role for ZBP-89 in the generation of the hematopoietic lineage. In contrast to our work, this group found that morpholino-mediated knockdown of ZBP-89 expression in zebrafish embryos resulted in nearly complete loss of primitive erythropoiesis, in addition to the reduction during definitive hematopoiesis which was observed in both studies. The reason for the discrepancy is not clear. There are several differences in technique that could potentially account for the disparate observations. One is the different morpholino constructs used. Li et al. utilized a morpholino construct that targets the translation start site (atgMO) of ZBP-89, whereas we used a morpholino targeting the splice donor site in exon 5 (resulting in an altered protein terminating before all four zinc fingers). Although it is not known whether maternal ZBP-89 transcripts are present in developing zebrafish embryos, an atgMO would inhibit translation of both maternally and zygotically derived ZBP-89 mRNA transcripts, whereas a splice site-targeted morpholino would disrupt only zygotically derived ZBP-89 mRNA transcripts. This could account for a more severe phenotype with the atgMO used by Li et al. However, the authors state that they also used a morpholino targeting the splice donor site in exon 8 (resulting in an altered protein terminating after the second zinc finger) and observed a similar phenotype, although these data are not shown. A second possibility is differences in the degree of ZBP-89 gene knockdown. It is possible that Li et al. achieved a greater overall reduction of ZBP-89 expression than we did in our experiments. We analyzed our ZBP-89 morphant embryos by RT-PCR and found markedly reduced levels of ZBP-89 full-length mRNA transcripts, although some residual expression remained (Fig. 3). Li et al. did not present data documenting their degree of ZBP-89 knockdown, so it is difficult to compare results. A third possibility is the timing of analysis. Li et al. analyzed their zebrafish embryos for hemoglobinized cells at 48 hours postfertilization (hpf), whereas we analyzed our embryos at 72 hpf. It is possible that dilution of the injected

morpholinos by 72 hpf could have resulted in a less severe phenotype, although the loss of thrombocytes that we observed was evident at 96 hpf.

In addition to the zebrafish experiments, our study included in vivo loss-of-function studies with mice using a ZBP-89 gene trap allele. The tetraploid complementation experiments shown in Fig. 5 support our conclusion that ZBP-89 is dispensable, or least functional at low levels, for primitive erythropoiesis. (As we discuss in the paper, the ZBP-89 gene trap allele produces low levels of full-length ZBP-89 mRNA transcripts, likely due to splicing around the gene trap vector.)

REFERENCES

1. **Bai, L., and J. L. Merchant.** 2000. Transcription factor ZBP-89 cooperates with histone acetyltransferase p300 during butyrate activation of p21waf1 transcription in human cells. J. Biol. Chem. **275:**30725–30733.
2. **Bai, L., and J. L. Merchant.** 2003. Transcription factor ZBP-89 is required for STAT1 constitutive expression. Nucleic Acids Res. **31:**7264–7270.
3. **Brand, M., J. A. Ranish, N. T. Kummer, J. Hamilton, K. Igarashi, C. Francastel, T. H. Chi, G. R. Crabtree, R. Aebersold, and M. Groudine.** 2004. Dynamic changes in transcription factor complexes during erythroid differentiation revealed by quantitative proteomics. Nat. Struct. Mol. Biol. **11:**73–80.
4. **Bresnick, E. H., M. L. Martowicz, S. Pal, and K. D. Johnson.** 2005. Developmental control via GATA factor interplay at chromatin domains. J. Cell. Physiol. **205:**1–9.
5. **Cantor, A. B., S. G. Katz, and S. H. Orkin.** 2002. Distinct domains of the GATA-1 cofactor FOG-1 differentially influence erythroid versus megakaryocytic maturation. Mol. Cell. Biol. **22:**4268–4279.
6. **Cantor, A. B., and S. H. Orkin.** 2005. Coregulation of GATA factors by the Friend of GATA (FOG) family of multitype zinc finger proteins. Semin. Cell Dev. Biol. **16:**117–128.
7. **Carroll, J. S., X. S. Liu, A. S. Brodsky, W. Li, C. A. Meyer, A. J. Szary, J. Eeckhoute, W. Shao, E. V. Hestermann, T. R. Geistlinger, E. A. Fox, P. A. Silver, and M. Brown.** 2005. Chromosome-wide mapping of estrogen receptor binding reveals long-range regulation requiring the forkhead protein FoxA1. Cell **122:**33–43.
8. **Chang, A. N., A. B. Cantor, Y. Fujiwara, M. B. Lodish, S. Droho, J. D. Crispino, and S. H. Orkin.** 2002. GATA-factor dependence of the multitype zinc-finger protein FOG-1 for its essential role in megakaryopoiesis. Proc. Natl. Acad. Sci. USA **99:**9237–9242.
9. **Crispino, J. D., M. B. Lodish, J. P. MacKay, and S. H. Orkin.** 1999. Use of altered specificity mutants to probe a specific protein-protein interaction in differentiation: the GATA-1:FOG complex. Mol. Cell **3:**219–228.
10. **Crispino, J. D., M. B. Lodish, B. L. Thurberg, S. H. Litovsky, T. Collins, J. D. Molkentin, and S. H. Orkin.** 2001. Proper coronary vascular development and heart morphogenesis depend on interaction of GATA-4 with FOG cofactors. Genes Dev. **15:**839–844.
11. **de Boer, E., P. Rodriguez, E. Bonte, J. Krijgsveld, E. Katsantoni, A. Heck, F. Grosveld, and J. Strouboulis.** 2003. Efficient biotinylation and single-step purification of tagged transcription factors in mammalian cells and transgenic mice. Proc. Natl. Acad. Sci. USA **100:**7480–7485.
12. **Dignam, J. D., R. M. Lebovitz, and R. G. Roeder.** 1983. Accurate transcription initiation by RNA polymerase II in a soluble extract from isolated mammalian nuclei. Nucleic Acids Res. **11:**1475–1489.
13. **Doyle, K., Y. Zhang, R. Baer, and M. Bina.** 1994. Distinguishable patterns of protein-DNA interactions involving complexes of basic helix-loop-helix proteins. J. Biol. Chem. **269:**12099–12105.
14. **Eggan, K., and R. Jaenisch.** 2003. Differentiation of F1 embryonic stem cells into viable male and female mice by tetraploid embryo complementation. Methods Enzymol. **365:**25–39.
15. **Eisbacher, M., M. L. Holmes, A. Newton, P. J. Hogg, L. M. Khachigian, M. Crossley, and B. H. Chong.** 2003. Protein-protein interaction between Fli-1 and GATA-1 mediates synergistic expression of megakaryocyte-specific genes through cooperative DNA binding. Mol. Cell. Biol. **23:**3427–3441.
16. **Elagib, K. E., F. K. Racke, M. Mogass, R. Khetawat, L. L. Delehanty, and A. N. Goldfarb.** 2003. RUNX1 and GATA-1 coexpression and cooperation in megakaryocytic differentiation. Blood **101:**4333–4341.
17. **Eng, J. K., A. L. McCormack, and J. R. Yates III.** 1994. An approach to correlate tandem mass spectral data of peptides with amino acid sequences in a protein database. J. Am. Soc. Mass Spectrom. **5:**976–989.
18. **Evans, T., and G. Felsenfeld.** 1989. The erythroid-specific transcription factor Eryf1: a new finger protein. Cell **58:**877–885.
19. **Fujiwara, Y., C. P. Browne, K. Cunniff, S. C. Goff, and S. H. Orkin.** 1996. Arrested development of embryonic red cell precursors in mouse embryos lacking transcription factor GATA-1. Proc. Natl. Acad. Sci. USA **93:**12355–12358.
20. **Gregory, R. C., D. J. Taxman, D. Seshasayee, M. H. Kensinger, J. J. Bieker, and D. M. Wojchowski.** 1996. Functional interaction of GATA1 with erythroid Kruppel-like factor and Sp1 at defined erythroid promoters. Blood **87:**1793–1801.
21. **Gregory, T., C. Yu, A. Ma, S. H. Orkin, G. A. Blobel, and M. J. Weiss.** 1999. GATA-1 and erythropoietin cooperate to promote erythroid cell survival by regulating bcl-xL expression. Blood **94:**87–96.
22. **Guyot, B., K. Murai, Y. Fujiwara, V. Valverde-Garduno, M. Hammett, S. Wells, N. Dear, S. H. Orkin, C. Porcher, and P. Vyas.** 2006. Characterization of a megakaryocyte-specific enhancer of the key hemopoietic transcription factor GATA1. J. Biol. Chem. **281:**13733–13742.
23. **Hollenhorst, P. C., A. A. Shah, C. Hopkins, and B. J. Graves.** 2007. Genome-wide analyses reveal properties of redundant and specific promoter occupancy within the ETS gene family. Genes Dev. **21:**1882–1894.
24. **Hong, W., M. Nakazawa, Y. Y. Chen, R. Kori, C. R. Vakoc, C. Rakowski, and G. A. Blobel.** 2005. FOG-1 recruits the NuRD repressor complex to mediate transcriptional repression by GATA-1. EMBO J. **24:**2367–2378.
25. **Huang, D. C., S. Cory, and A. Strasser.** 1997. Bcl-2, Bcl-XL and adenovirus protein E1B19kD are functionally equivalent in their ability to inhibit cell death. Oncogene **14:**405–414.
26. **Ishida, Y., J. Levin, G. Baker, P. E. Stenberg, Y. Yamada, H. Sasaki, and T. Inoue.** 1993. Biological and biochemical characteristics of murine megakaryoblastic cell line L8057. Exp. Hematol. **21:**289–298.
27. **Karnovsky, M. J., and L. Roots.** 1964. A direct colouring thiocholine method for cholinesterases. J. Histochem. Cytochem. **12:**219–221.
28. **Lai, J. S., and W. Herr.** 1992. Ethidium bromide provides a simple tool for identifying genuine DNA-independent protein associations. Proc. Natl. Acad. Sci. USA **89:**6958–6962.
29. **Law, D. J., M. Du, G. L. Law, and J. L. Merchant.** 1999. ZBP-99 defines a conserved family of transcription factors and regulates ornithine decarboxylase gene expression. Biochem. Biophys. Res. Commun. **262:**113–120.
30. **Letting, D. L., Y. Y. Chen, C. Rakowski, S. Reedy, and G. A. Blobel.** 2004. Context-dependent regulation of GATA-1 by friend of GATA-1. Proc. Natl. Acad. Sci. USA **101:**476–481.
31. **Li, Q., X. Fang, I. Olave, H. Han, M. Yu, P. Xiang, and G. Stamatoyannopoulos.** 2006. Transcriptional potential of the gamma-globin gene is dependent on the CACCC box in a developmental stage-specific manner. Nucleic Acids Res. **34:**3909–3916.
32. **Lin, H. F., D. Traver, H. Zhu, K. Dooley, B. H. Paw, L. I. Zon, and R. I. Handin.** 2005. Analysis of thrombocyte development in CD41-GFP transgenic zebrafish. Blood **106:**3803–3810.
33. **Martin, D. I., and S. H. Orkin.** 1990. Transcriptional activation and DNA binding by the erythroid factor GF-1/NF-E1/Eryf 1. Genes Dev. **4:**1886–1898.
34. **Merchant, J. L., G. R. Iyer, B. R. Taylor, J. R. Kitchen, E. R. Mortensen, Z. Wang, R. J. Flintoft, J. B. Michel, and R. Bassel-Duby.** 1996. ZBP-89, a Kruppel-like zinc finger protein, inhibits epidermal growth factor induction of the gastrin promoter. Mol. Cell. Biol. **16:**6644–6653.
35. **Merika, M., and S. H. Orkin.** 1995. Functional synergy and physical interactions of the erythroid transcription factor GATA-1 with the Kruppel family proteins Sp1 and EKLF. Mol. Cell. Biol. **15:**2437–2447.
36. **Mortensen, R. M., D. A. Conner, S. Chao, A. A. Geisterfer-Lowrance, and J. G. Seidman.** 1992. Production of homozygous mutant ES cells with a single targeting construct. Mol. Cell. Biol. **12:**2391–2395.
37. **Muntean, A. G., and J. D. Crispino.** 2005. Differential requirements for the activation domain and FOG-interaction surface of GATA-1 in megakaryocyte gene expression and development. Blood **106:**1223–1231.
38. **Muntean, A. G., Y. Ge, J. W. Taub, and J. D. Crispino.** 2006. Transcription factor GATA-1 and Down syndrome leukemogenesis. Leuk. Lymphoma **47:**986–997.
39. **Nichols, K. E., J. D. Crispino, M. Poncz, J. G. White, S. H. Orkin, J. M. Maris, and M. J. Weiss.** 2000. Familial dyserythropoietic anaemia and thrombocytopenia due to an inherited mutation in GATA1. Nat Genet. **24:**266–270.
40. **Pal, S., A. B. Cantor, K. D. Johnson, T. B. Moran, M. E. Boyer, S. H. Orkin, and E. H. Bresnick.** 2004. Coregulator-dependent facilitation of chromatin occupancy by GATA-1. Proc. Natl. Acad. Sci. USA **101:**980–985.
41. **Peng, J., and S. P. Gygi.** 2001. Proteomics: the move to mixtures. J. Mass Spectrom. **36:**1083–1091.
42. **Pevny, L., C. S. Lin, V. D'Agati, M. C. Simon, S. H. Orkin, and F. Costantini.** 1995. Development of hematopoietic cells lacking transcription factor GATA-1. Development **121:**163–172.
43. **Pevny, L., M. C. Simon, E. Robertson, W. H. Klein, S. F. Tsai, V. D'Agati, S. H. Orkin, and F. Costantini.** 1991. Erythroid differentiation in chimaeric mice blocked by a targeted mutation in the gene for transcription factor GATA-1. Nature **349:**257–260.
44. **Rechsteiner, M., and S. W. Rogers.** 1996. PEST sequences and regulation by proteolysis. Trends Biochem. Sci. **21:**267–271.
45. **Rodriguez, P., E. Bonte, J. Krijgsveld, K. E. Kolodziej, B. Guyot, A. J. Heck, P. Vyas, E. de Boer, F. Grosveld, and J. Strouboulis.** 2005. GATA-1 forms distinct activating and repressive complexes in erythroid cells. EMBO J. **24:**2354–2366.
46. **Sambrook, J., and D. W. Russell (ed.).** 2001. Molecular cloning: a laboratory manual, 3rd ed. Cold Spring Harbor Laboratory Press, Cold Spring Harbor, NY.
47. **Shevchenko, A., M. Wilm, O. Vorm, and M. Mann.** 1996. Mass spectrometric sequencing of proteins silver-stained polyacrylamide gels. Anal. Chem. **68:**850–858.

48. **Shivdasani, R. A., Y. Fujiwara, M. A. McDevitt, and S. H. Orkin.** 1997. A lineage-selective knockout establishes the critical role of transcription factor GATA-1 in megakaryocyte growth and platelet development. EMBO J. **16:**3965–3973.
49. **Takeuchi, A., Y. Mishina, O. Miyaishi, E. Kojima, T. Hasegawa, and K. Isobe.** 2003. Heterozygosity with respect to Zfp148 causes complete loss of fetal germ cells during mouse embryogenesis. Nat Genet. **33:**172–176.
50. **Tevosian, S. G., K. H. Albrecht, J. D. Crispino, Y. Fujiwara, E. M. Eicher, and S. H. Orkin.** 2002. Gonadal differentiation, sex determination and normal Sry expression in mice require direct interaction between transcription partners GATA4 and FOG2. Development **129:**4627–4634.
51. **Trainor, C. D., J. G. Omichinski, T. L. Vandergon, A. M. Gronenborn, G. M. Clore, and G. Felsenfeld.** 1996. A palindromic regulatory site within vertebrate GATA-1 promoters requires both zinc fingers of the GATA-1 DNA-binding domain for high-affinity interaction. Mol. Cell. Biol. **16:**2238–2247.
52. **Tsai, S. F., D. I. Martin, L. I. Zon, A. D. D'Andrea, G. G. Wong, and S. H. Orkin.** 1989. Cloning of cDNA for the major DNA-binding protein of the erythroid lineage through expression in mammalian cells. Nature **339:**446–451.
53. **Tsang, A. P., Y. Fujiwara, D. B. Hom, and S. H. Orkin.** 1998. Failure of megakaryopoiesis and arrested erythropoiesis in mice lacking the GATA-1 transcriptional cofactor FOG. Genes Dev. **12:**1176–1188.
54. **Tsang, A. P., J. E. Visvader, C. A. Turner, Y. Fujiwara, C. Yu, M. J. Weiss, M. Crossley, and S. H. Orkin.** 1997. FOG, a multitype zinc finger protein, acts as a cofactor for transcription factor GATA-1 in erythroid and megakaryocytic differentiation. Cell **90:**109–119.
55. **Vernimmen, D., M. De Gobbi, J. A. Sloane-Stanley, W. G. Wood, and D. R. Higgs.** 2007. Long-range chromosomal interactions regulate the timing of the transition between poised and active gene expression. EMBO J. **26:**2041–2051.
56. **Vyas, P., K. Ault, C. W. Jackson, S. H. Orkin, and R. A. Shivdasani.** 1999. Consequences of GATA-1 deficiency in megakaryocytes and platelets. Blood **93:**2867–2875.
57. **Vyas, P., M. A. McDevitt, A. B. Cantor, S. G. Katz, Y. Fujiwara, and S. H. Orkin.** 1999. Different sequence requirements for expression in erythroid and megakaryocytic cells within a regulatory element upstream of the GATA-1 gene. Development **126:**2799–2811.
58. **Wadman, I. A., H. Osada, G. G. Grutz, A. D. Agulnick, H. Westphal, A. Forster, and T. H. Rabbitts.** 1997. The LIM-only protein Lmo2 is a bridging molecule assembling an erythroid, DNA-binding complex which includes the TAL1, E47, GATA-1 and Ldb1/NLI proteins. EMBO J. **16:**3145–3157.
59. **Weiss, M. J., G. Keller, and S. H. Orkin.** 1994. Novel insights into erythroid development revealed through in vitro differentiation of GATA-1 embryonic stem cells. Genes Dev. **8:**1184–1197.
60. **Weiss, M. J., C. Yu, and S. H. Orkin.** 1997. Erythroid-cell-specific properties of transcription factor GATA-1 revealed by phenotypic rescue of a gene-targeted cell line. Mol. Cell. Biol. **17:**1642–1651.
61. **Welch, J. J., J. A. Watts, C. R. Vakoc, Y. Yao, H. Wang, R. C. Hardison, G. A. Blobel, L. A. Chodosh, and M. J. Weiss.** 2004. Global regulation of erythroid gene expression by transcription factor GATA-1. Blood **104:**3136–3147.
62. **Wu, Y., X. Zhang, M. Salmon, and Z. E. Zehner.** 2007. The zinc finger repressor, ZBP-89, recruits histone deacetylase 1 to repress vimentin gene expression. Genes Cells **12:**905–918.
63. **Xu, Z., X. Meng, Y. Cai, H. Liang, L. Nagarajan, and S. J. Brandt.** 2007. Single-stranded DNA-binding proteins regulate the abundance of LIM domain and LIM domain-binding proteins. Genes Dev. **21:**942–955.
64. **Zhang, X., I. H. Diab, and Z. E. Zehner.** 2003. ZBP-89 represses vimentin gene transcription by interacting with the transcriptional activator, Sp1. Nucleic Acids Res. **31:**2900–2914.